Programme Area: Carbon Capture and Storage

Project: Storage Appraisal

Title: Exemplar Modelling and Dynamic Simulation of Bunter Fm Sst Closures

Abstract:

This document is a supporting document to deliverable MS6.1 UK Storage Appraisal Final Report.

Context:

This £4m project produced the UK's first carbon dioxide storage appraisal database enabling more informed decisions on the economics of CO2 storage opportunities. It was delivered by a consortium of partners from across academia and industry - LR Senergy Limited, BGS, the Scottish Centre for Carbon Storage (University of Edinburgh, Heriot-Watt University), Durham University, GeoPressure Technology Ltd, Geospatial Research Ltd, Imperial College London, RPS Energy and Element Energy Ltd. The outputs were licensed to The Crown Estate and the British Geological Survey (BGS) who have hosted and further developed an online database of mapped UK offshore carbon dioxide storage capacity. This is publically available under the name CO2 Stored. It can be accessed via www.co2stored.co.uk.

UKSAP

Appendix A5.6

Exemplar Modelling and Dynamic Simulation of Bunter Sandstone Formation Closures in the Southern North Sea

Conducted for

The Energy Technologies Institute

By

British Geological Survey

Heriot-Watt University

Authors	Michelle Bentham, John Williams & Sarah Hannis, Min Jin, Gillian Pickup
Technical Audit	Sam Holloway & Eric Mackay
Quality Audit	
Release to Client	Grahame Smith
Date Released	28th October 2011 (final)

File Location
Appendix A5.6 - Exemplar Modelling & Dynamic Simulation of Bunter Sandstone Formation Closures in the SNS.doc

Executive Summary

The aim of this work was to build a 3D geocellular model of the reservoir and sealing formations for a closure in the Bunter Sandstone Formation which could be used to model CO_2 injection.

A region in storage unit 139.000 (zone 4 Bunter Sandstone Formation) of 44.0 km by 25.2 km was chosen for detailed modelling. The target daughter storage unit 139.016 (Bunter closure 36) was chosen for modelling as:

- No faulting was visible on the seismic over the closure

- The storage capacity was estimated to be large enough to store a sizable amount of CO_2

- The area included three additional closures (storage units 139.017, 139.018 and 139.019) that could be used to study the impact of CO_2 injection on adjacent storage units

- Data coverage was good over the chosen area

The static geocellular model was constructed by BGS in PETREL^{TM} (Schlumberger,2010a) using PGS seismic surfaces, IHS well tops (from the EDIN database), well logs (for 12 wells) and core data for one well.

The Bunter Sandstone Formation was divided into five reservoir Petrel-zones comprised of varying fluvial facies based on the depositional environment. These could be correlated across the model using geophysical logs. Each Petrel-zone contained a distinct distribution of three lithologies (sandstone, cemented sandstone and shale). An apparently continuous (correlatable) layer of impermeable cemented sandstone at the top of the fourth petrel-zone almost splits the Bunter Sandstone Formation reservoir in two.

The grid had approximately 450 000 cells, of length and breadth 400m in the horizontal plane. The cell thickness varied from 24 m to 0.5 m in the sandstone.

Lithologies were distributed through the model using stochastic techniques and porosity values for each lithology type were determined from well logs and used to generate a stochastic distribution. Permeability values were taken from cross-plots of porosity and permeability values from core plugs in the Bunter Sandstone Formation and distributed stochastically throughout the model but tied to the porosity values. The average porosity of the sandstone was 18%, and the geometric average of the permeability was approximately 10 mD. The shales were given a constant porosity of 2.7% and an average permeability value of 0.0065 mD, while the cemented sandstones were given a constant value of zero for both porosity and permeability. The geocellular model generated in PETREL^{TM} was exported to the ECLIPSE^{TM} simulation software package (Schlumberger, 2010b) for dynamic modelling of CO_2 injection.

Supercritical CO_2 was injected into the model using 10 vertical wells which were completed throughout the top four Petrel zones of the Bunter Sandstone Formation. The wells were therefore injecting both above and below the impermeable cemented sandstone layer. In the

base case model CO_2 was injected only into Closure 36, but various other scenarios and sensitivities were investigated, including injection into two or three closures either simultaneously or sequentially.

The target well injection rate was set at 2 Mt/yr, but this was subject to the standard project assumption that pressures should not exceed 90% of the fracture pressure at the appropriate depth. A limit was also needed on migration of free CO_2 from the dome via the spill point, and this was taken to be a cumulative 0.01% of the total injected CO_2 by mass.

Due to the large uncertainty in reservoir properties a range of scenarios was simulated, including modifying the boundary conditions, and the heterogeneity. The results were combined to give minimum, most likely and maximum values for the pore volume utilisation, the sweep efficiency and the capacity in Mt. The table below summarises the results from the Exemplar simulations.

	Minimum	Most Likely	Maximum
Pore Volume Utilisation (%)	4	19	33
Sweep Efficiency (%)	12	33	65
Storage Capacity (Mt)	70	331	484

The amount of CO_2 which can be stored in a particular closure is reduced when CO_2 is injected into multiple domes, due to pressure build-up. The sensitivity studies showed that the PV utilisation decreased when the model size was reduced, in agreement with other studies. The heterogeneity in the model was found to have a significant effect on the results. The model contained many shales and cemented sandstones, and there was one layer of cemented sandstone which crossed most of the model. The effect of removing the cemented layer increased the PV utilisation, as expected, and a homogeneous model.

Some important findings arose from this study.

- The storage capacity may be controlled by either the pressure (when the pressure increases above the maximum limit, the rate must be reduced), or the migration rate (if a high injection rate is maintained, CO_2 will reach the spill point more rapidly).

- The pore volume utilisation and total capacity are quite sensitive to the assumed value for the fracture pressure gradient. A change in this gradient may switch the storage control from pressure-controlled to rate-controlled.

- The storage capacity for an open model may be less than that for a closed system, if heterogeneity encourages a low pore volume utilisation.

- It is import to monitor the pressure at the crest of a dome. Even when the injection rate is pressure controlled at the depth of the well completions, the pressure may rise above a safe limit in the crest.

- It may be possible to increase storage capacity by controlling the injection rate. A lower rate will allow CO_2 more time to rise buoyantly and to dissolve in brine, before reaching the spill point.

Contents

List of Tables

List of Figures

1   Introduction

The work undertaken forms part of work package 4 of the UK Storage Appraisal Project (UKSAP).

The Bunter Sandstone Formation and its structural closures were identified in UKSAP as storage units that have the potential to store CO_2. Due to the large storage potential of the Bunter Sandstone Formation and the presence within it of large mappable saline water-bearing closures it was targeted as an exemplar for dynamic modelling of CO_2 injection. This particular study is known as Exemplar 2. The aim of Exemplar 2 was to investigate an individual closure in the Bunter Sandstone Formation and model CO_2 injection into it. As well as modelling the target closure, an area outside the closure was assessed in order to model pressure effects and influence on the storage capacity of 'neighbouring closures'. Using a closed structure in the Bunter Sandstone Formation for storage has the advantage of the CO_2 being confined within a known area, with the additional advantage of the closure being connected to the wider Bunter Sandstone Formation pore space, which in the long term may allow brine displacement and pressure dissipation.

BGS was tasked to provide an auditable and defensible geocellular model of a Bunter Sandstone Formation closure to Heriot-Watt University for use in CO_2 injection simulation using the ECLIPSE300 simulator. Restrictions in run time and computing resources meant that the geocellular model was limited to ~450 000 grid cells. Due to time, computing and data restrictions, faults were not included in the model area. The geocellular model constructed in PETREL had to reflect the geology of the reservoir unit (Bunter Sandstone Formation) as well as including the overburden (Haisborough Group) and underburden (Bunter Shale Formation).The geocellular model was to focus on one 'target' closure, but one or two additional closures were to be included in the modelled area so that pressure interference between injection projects in adjacent domes could be investigated.

2   Model Area

The Bunter Sandstone Formation in the UK sector of the southern North Sea (SNS) was mapped in UKSAP using a combination of PGS depth surfaces, (interpreted by PGS on the SNS MegaMerge 3D seismic survey and gridded at 1000 x 1000 m) and IHS well data. Although there is good seismic data coverage over the whole of the Bunter Sandstone Formation, the PGS data do not cover the full extent of the formation. In areas outside of the PGS data coverage, the Bunter Sandstone Formation surface was gridded using formation tops from the IHS well database (**Figure A2.1**). No structural data (e.g. location of faults and salt walls) were available to this project.
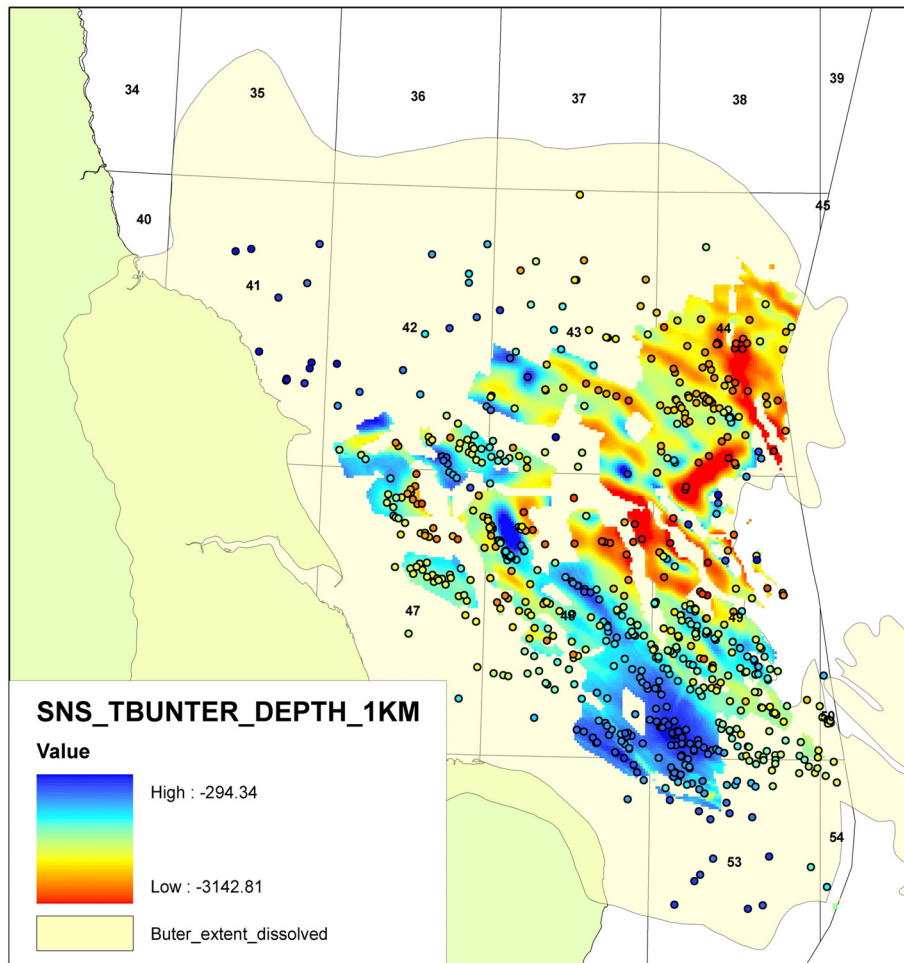
Figure A2.1: Location of PGS surface data and IHS wells tops for the Bunter Sandstone Formation in the southern North Sea

On request of the UKSAP project board the Bunter Sandstone Formation was divided into zones based on geological features as boundaries, such as salt walls and fault zones. However the Bunter Sandstone Formation is known to be hydrostatically pressured and it is unlikely that the formation is compartmentalised on geological timescales. Within each zone it was possible to map individual closed structures or traps.

Following a review of all of the mapped closures a single 'target' closure was identified for the exemplar modelling work based on the following criteria:

- Considered to be un-faulted within the detection limits of the PGS MegaMerge data

- Good PGS data coverage over the whole structure

- A complete cap rock/seal over the above the target structure

- Presence of nearby closures in order to investigate interactions during CO_2 injection

- The crest of the target closure should be deeper than 800 m

The final target closure was selected from 29 structural closures identified within the extent of the available project data. The closures were 'risked' using the data available in UKSAP. Of the 29 closures only 10 closures appeared to be un-faulted. The 'potentially' un-faulted closures are indicated in green on **Figure A2.2** (Raistrick et al. 2011). Most of the un-faulted closures lie within Zone 4 (CarbonStore storage unit ID 139.000) of the Bunter Sandstone Formation. As a result, this area was investigated to indentify a 'target' closure for the exemplar modelling. The centroid depth (Holloway et al. 2011) of the Bunter Sandstone Formation in Zone 4 is 1591 m. The formation crops out at the sea bed in well 43/28a- 03. The zone is bounded to the north and east by fault zones, to the south by salt walls, and to the west by a combination of both salt walls and subcrop.
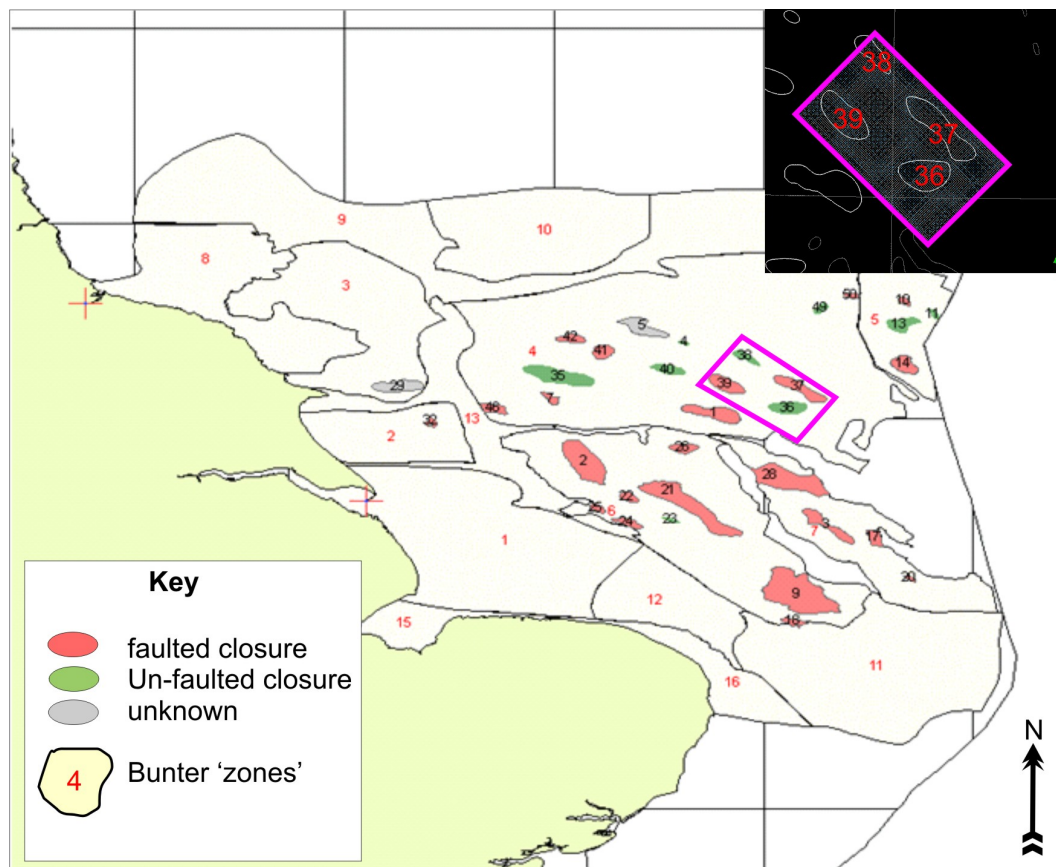
Figure A2.2 Mapped zones and closures in the Bunter Sandstone Formation

The selection criteria were largely met by a cluster of domes in the southwest area of zone 4 (**Figure A2.2**). The closures within this area are 36, 37, 38 and 39 (CarbonStore storage unit IDs 139.016, 139.017, 139.018 and 139.019 respectively). All of the closures in the model area are simple anticlinal structures elongated to the NW-SE, formed by the movement of the underlying Zechstein Group salts.

Further investigation revealed closure 36 to be the best candidate for the 'target' closure. It appears to be un-faulted (on the PGS MegaMerge seismic data), has fairly good data coverage and is in close proximity to closures 37, 38 and 39, which could be included in the model area to investigate the effect of CO_2 injection on neighbouring closures. The Bunter Sandstone Formation in the model area ranges from between 174 and 274 m thick, and lies at a depth of 767 and 2934 m. The thickness of the Bunter Sandstone Formation at the crest of closure 36 is 217 m (well 44/26- 01), and the top of the formation is at 1186 m depth.

The greatest uncertainty relating to closure 36 is the thickness of the saliferous mudstones of the Haisborough Group which forms the primary cap rock to the Bunter Sandstone Formation. At the crest of closure 36 it is 308 m thick (well 44/26- 01). However, the seal thickness varies between 44 and 826 m over the whole of the model area. It is particularly thin to the southeast of closure 36 where it has been eroded by the Base Cretaceous Unconformity.

Closure 38 has been cut by the boundaries of the model area so appears to be open to the NW, but it is closed to the NW outside of the model area based on the PGS depth map of the top Bunter Sandstone Formation. The full extent of closure 38 was not included in the model are due to restrictions on the amount of the data available to project. It was considered more important to leave a boundary around closure 36 than include all of closure 38 and cut the boundary of the model too close to the SE edge of closure 36. Closure 38 is only partially covered by the PGS MegaMerge, as this is not the target structure it was decided that it would be satisfactory to interpolate the top Bunter Sandstone Formation depth grid in this area.

The coordinates of the chosen model area are shown in **Table A2.1**. The region is approximately 44.0 km by 25.2 km.

x	y
430540	6023200
462160	5991800
443120	5972700
411520	6004250

Table A2.1: Coordinates of the model area (UTM zone 31)

3   Data

The geocellular model was constructed in PETREL^{TM} using depth grids of the relevant surfaces provided by PGS, wireline logs from IHS and well tops from the IHS EDIN^{TM} database augmented with additional data from BGS databases. The IHS wireline log data available is recorded in **Table A3.1** and the PGS data is listed below:

- 100 m increment depth grid of the Top Bunter Sandstone Formation

- 100 m increment depth grid of the Top Triassic (Top Haisborough Group)

- 100 m increment depth grid of the Base Cretaceous Unconformity

- Seismic edge map of the Top Bunter Sandstone Formation

Wells	Geophysical logs available	Core analysis
43/25-1	CALI DRHO DT GR ILD ILM INTT NPHI POTA RHOB THOR URAN -- 194 - 16140	
44/21-1	CALI DT GR ILD INTT LL7 LL8 LN NEUT SN SP -- 710 - 14130	
44/21-2	CALI CGR DRHO DT GR ILD INTT MSFL NPHI PEF POTA RHOB SFLU SGR SP THOR URAN -- 3.5 - 15279.5	
44/21a-10	AC CAL CNC GR GRD K PE RILD RILM RIPD RIPM TH TTEN TTEND U ZCOR ZDEN -- 35 - 13865	
44/21a-9	AC CAL CALR CNC GR GRD PE RILD RILM RIPD RIPM TTEN TTEND ZCOR ZDEN -- 100 - 14041	
44/26-1	CALI DRHO DT GR ILD INTT LL7 RHOB SN SP -- 496 - 5066	available
44/26-2	CALI DRHO DT GR IL ILD INTT NPHI RHOB -- 322 - 13585	
44/26-3	AC CAL CNC CORR DEN GR K RILD RILM TH TTEN U -- 2394.5 - 13888	
44/26-4	CALI CALS CGR DRHO DT GR ILD ILM INTT NPHI PEF POTA RHOB SFLU SGR TENS THOR URAN -- 295 - 16185	
44/26c-6	AT10 AT20 AT30 AT60 AT90 CAL1 CAL2 CALI CALS CGR DRHO DT DTL DTLF DTLN EATT FVD FVU GR HTEN IDER ILD ILM IMER NPHI PEF POTA RHOB SA SGR TENS THOR TPL TPRA TURA UPRA URAN -- 81.5 - 15450	
44/27-1	CALI CGR DRHO DT DTL GR ILD ILM INTT LLD LLG LLS MSFL NPHI PEF POTA RHOB SFLU SGR SP THOR URAN -- 348 - 16520	
44/27-2	CALI CGR DRHO DT DTL GR ILD ILM INTT NPHI PEF POTA RHOB SGR TENS THOR URAN -- 203.1 - 14791.4004	
49/01-3	CALI CGR DRHO DT DTL GR HTEN ILD ILM INTT LDTL LSDT NPHI PEF POTA RHOB SFLU SGR SP TENS THOR URAN -- 198 - 16166	

Table A3.1: Wells used in the model (sourced from IHS)

In addition a small area of 3D seismic data over dome 36 was available to investigate faulting and to test model robustness (**Table A3.2**).

x	y
434600	5994840
449625	5994160
449290	5983990
434450	5984620

Table A3.2: Coordinates of the 3D seismic data covering closure 36 (UTM zone 31)

4   Geological Description of the Reservoir and Sealing Formations

4.1   Bunter Sandstone Formation

The Bunter Sandstone Formation in the UK sector of the southern North Sea (SNS) is a large predominantly saline water-bearing formation which extends east into the Dutch Sector of the SNS and beyond. It outcrops onshore in the UK where it is known as the Sherwood Sandstone Group, and continues into the Irish Sea where it is known as the Ormskirk Sandstone Formation.

The Triassic Bunter Sandstone Formation in the SNS was deposited in a fluvial environment (Ketter 1991), and is interpreted to be a series of coalescing alluvial fans dissected by fluvial braided channels deposited in an arid to semi-arid environment (Bifani, 1986). The low sinuosity channels transect a broad low relief alluvial braidplain (Ritchie and Pratsides, 1993). The sediment is derived from the west-southwest and is thought to drain into a playa lake in the north and northeast (Ritchie and Pratsides, 1993). The domal structures which form the Bunter closures and the traps for several gas accumulations in the SNS have been formed by the movement of the underlying Zechstein Group evaporites (**Figure A4.1**).

In the East Irish Sea Basin and the SNS the Bunter Sandstone Formation acts as the reservoir for several hydrocarbon fields, while onshore in the UK it is utilised for potable water. The Esmond gas complex lies 43 km to the north of closure 36. The Caister B gas field is the closest hydrocarbon accumulation to closure 36.
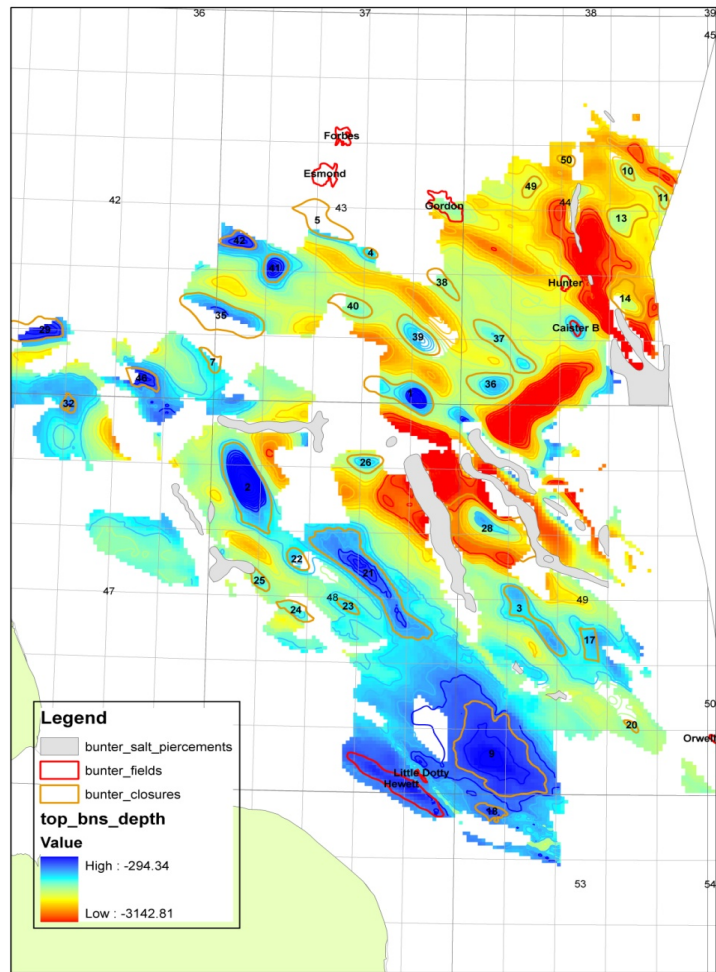
Figure A4.1 Closures and gas fields in the Bunter Sandstone Formation and PGS MegaMerge top Bunter Sandstone Formation depth surface

The Bunter Sandstone Formation has been divided into lithofacies by a number of authors. Bifani (1986) suggested a subdivision of the Bunter Sandstone Formation based on wells in the Esmond gas complex. This was later refined by Ketter (1991). Ritchie and Pratsides (1993) divided the Bunter Sandstone based on wells in the Caister B gas field. These broad divisions have formed a guide for subdividing the Bunter Sandstone Formation in the model area into petrel-zones based on well interpretation, sedimentary facies interpretations and reservoir properties. The reservoir divisions suggested by Bifani, Ketter and Ritchie vary slightly, and have been modified based here on the basis of the data available from the model area. Each gas field is interpreted to be in a different part of the fluvial system, and the same is also true of closure 36 (**Table A4.1**).

Location	Facies	Reference
Esmond	Major channel facies in the mid fan area	Bifani 1983
Forbes	Rapidly shifting, fluvial braided streams in the mid fan area, prograding over broader channels and sheetflood alluvial plain deposits in the lower fan area	Bifani 1983
Gordon	More distal (lower fan) deposits with some thin channel deposits	Bifani 1983
Caister	Distal flood plain setting, flood plain setting with two distinct channel units	Ritchie 1993
Closure 36	Lies to the south of the gas fields and considering the sediment transport direction it is likely dome 36 is more proximal in the fluvial system than Esmond, Forbes, Gordon and Caister.	

Table A4.1 Facies within the Bunter Sandstone Formation

4.2   Haisborough Group

The Haisborough Group forms the primary seal to the Bunter Sandstone Formation, and comprises of a series of mudstones and evaporites. The group was deposited in a subsiding onshore basin in a distal floodplain setting. Evaporites were deposited during intermittent, widespread marine incursions across the basin. The Haisborough Group is divided into three formations. The lowermost is the Dowsing Dolomite Formation which consists mostly of red silty mudstones. The Dowsing Dolomite Formation also includes the Röt Halite Member which acts as a major seal for the Bunter Sandstone Formation, and below that, the Solling Mudstone which lies immediately above the Bunter Sandstone Formation. The Dudgeon Saliferous Formation overlies the Dowsing Dolomite which consists of thick, predominantly green mudstones up to 100 m thick. The Keuper Halite forms the boundary between the Dudgeon Saliferous Formation and the overlying Triton Anhydritic Formation. The Triton Anhydritic Formation consists of a monotonous sequence of red mudstone with a few layers of anhydrite that form the Keuper Anhydritic Member.

The thickness of the Haisborough Group in the model area is controlled by the Base Cretaceous Unconformity which cuts down into the Haisborough Group in the southeast of the model area. The seal thickness is greatly reduced in this area from a maximum 826 m to 44 m in the SE of the model area (**Figure A4.2**). At the crest of closure 36 the seal thickness is 308 m.
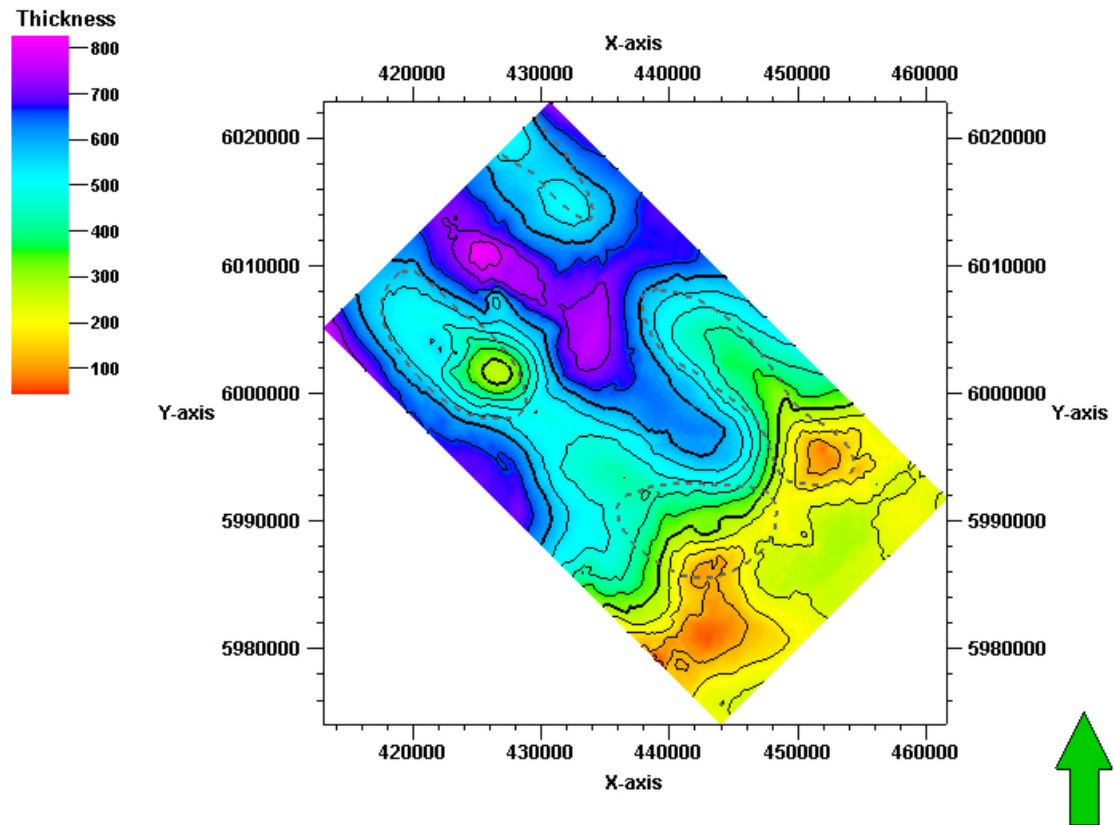
Figure A4.2 Thickness of the upper seal (Haisborough Group) in the model area

4.3   Bunter Shale Formation

The Bunter Shale Formation comprises mostly of red or red-brown silty mudstones with thin intercalations of siltstones and a few beds of dolomite. Its thickness is regionally consistent across the basin. It was deposited in a playa lake or inland sea (Glennie 1998). The average thickness of the Bunter Shale Formation in the model area is 387 m.

5 Framework Geological Model and Layering

The framework geological model was built in PETREL using its structural modelling processes. The framework model is made up of a series of horizons generated from surfaces (provided by PGS) and well tops (provided by IHS). The Chalk Group, Cromer Knoll Group and Jurassic were added for geological context and have no geological properties assigned to them (**Table A5.1**).

Surface	Data source	Comments
Top Chalk Group	PGS depth surface	Used for geological context
Top Cromer Knoll	IHS well tops	Used for geological context
Base Cretaceous Unconformity (top Haisborough Group in part)	PGS depth surface	Top of the dynamic model and top of the cap rock
Top Triassic (top Haisborough Group)	PGS depth surface & base Cretaceous depth surface	Top of the dynamic model and top of the main cap rock
Top Rot Halite Member	IHS well tops	Cap rock
Top Solling Mudstone	BGS well interpretation	Top of the primary cap rock
Top Bunter Sandstone Formation	PGS depth surface	Storage unit (reservoir)
Top Bunter Shale Formation	IHS well tops	Base of storage unit and top of underlying cap rock
Base Bunter Shale	IHS well tops	Base of underlying cap rock

Table A5.1 Horizons within the geocellular model

The volumes between the horizons were subdivided into units defined as zones in PETREL but for the purpose of this study will be referred to as petrel-zones.

The Bunter Sandstone Formation was sub-divided into 5 petrel-zones. The overlying cap rock (Haisborough Group) was split into 3 petrel-zones, while the Bunter Shale Formation was added as an additional petrel-zone to represent the underlying seal.
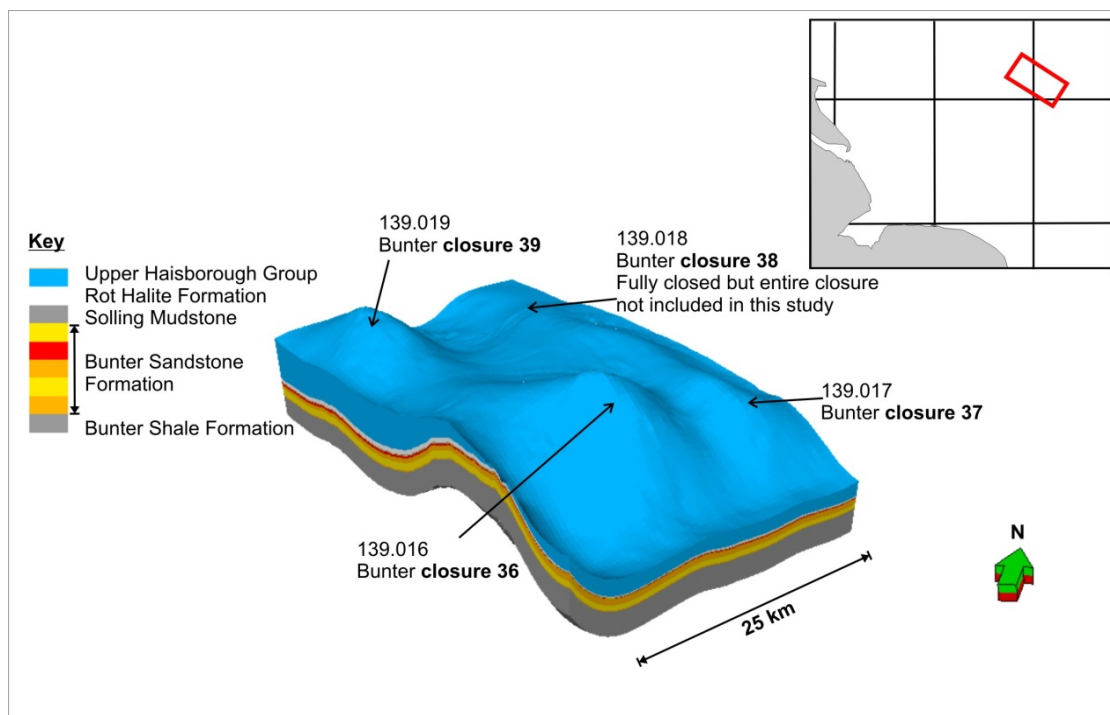
Figure A5.1 Petrel-zones in the model

Each petrel-zone was then layered individually based on geology to reflect the facies and properties interpretation for each petrel-zone. The number of layers and layer spacing in each petrel-zone was chosen to incorporate the level of detail required in the cap rock and reservoir whilst keeping the number of cells within the specified limits.

5.1 Haisborough Group Layering

The Haisborough Group is represented by three petrel-zones based on the geology and requirements for the final use of the model (modelling the injection of CO_2). The lower section of the Haisborough group will act as the top seal to the Bunter Sandstone Formation reservoir. As a result more detail was required to accurately represent the geology of the lower section of the Haisborough Group.

The geological unit directly overlying the Bunter Sandstone Formation is the Solling Mudstone (equivalent of the Solling Claystone or in some wells the Röt Shale). It was picked in all of the wells in the model area using gamma ray and sonic logs. In the model area the Solling Mudstone has an average thickness of 12 m. It is composed of red, silty mudstones and is sometimes overlain by thin deltaic sandstones (Cameron et al 1992), although these do not occur in the model area. The Solling Mudstone was subdivided into 2 layers to allow investigation of the capillary entry pressure effects at the base of the caprock during dynamic modelling. In order to facilitate this, a thin layer corresponding in thickness to those layers at the top of the reservoir was inserted at the base of the Solling Mudstone. Overlying the Solling Mudstone is the Röt Halite Member. This is potentially an important seal above the Bunter Sandstone Formation because it likely has close to zero permeability if unfractured. It was easily picked on the wells (**Figure A5.2**) because of its distinctive log response. The Röt Halite is modelled as a single layer within the cap rock succession. The remainder of the overlying Haisborough Group was incorporated into an additional layer within the model, representing the mudstones and evaporites of the Dowsing Dolomite Formation, the Dudgeon Saliferous Formation and the Triton Anhydritic Formation.

The characteristic geophysical log signatures of the three modelled sub-divisions in the Haisborough Group are shown in **Figure A5.2**.
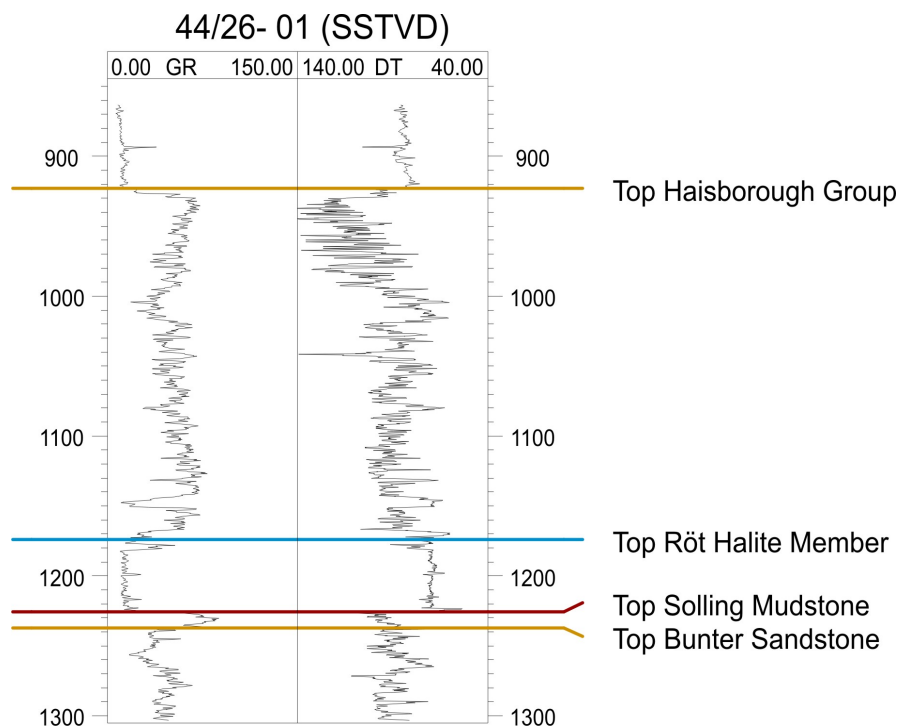
Figure A5.2 Well log and interpretation for the Haisborough Group

5.2   Bunter Sandstone Formation Layering

The Bunter Sandstone in the model area was split into 5 petrel-zones, based on the interpreted depositional environment derived from literature, and the well data (see section 4.2). Using wireline logs, (primarily gamma ray, sonic and density), each petrel-zone was split into a number of layers. The layering aimed to:

- Keep the overall number of model cells within the specified limit

- Ensure that the geology was reflected in sub-layers, broadly guided by the interpreted facies, e.g. the sub-layer thickness in zone 3 was 2.5 m on average to ensure that thinner interbedded shales were represented in the model.

Care was taken to accurately represent the shale layers within the model area. In the Caister B Field (Ritchie and Pratsides 1993), formation pressure tests show that the shales form effective pressure barriers and affect bottom water drive. Halite cemented layers also form vertical permeability barriers which impede bottom water drive. These halite cements are also found to reduce vertical permeability in the Esmond field (Bifani 1986). If water influx is impeded by these barriers it is likely that they will also act as vertical barriers to CO_2 flow in the Bunter Sandstone Formation. Cemented horizons were recognised in the wells in the model area. To ensure that the shale and cemented sandstone horizons appeared in the facies model the layer thickness was reduced in regions which related to the thickness of the shale and cemented sandstone lithologies from the well interpretations.
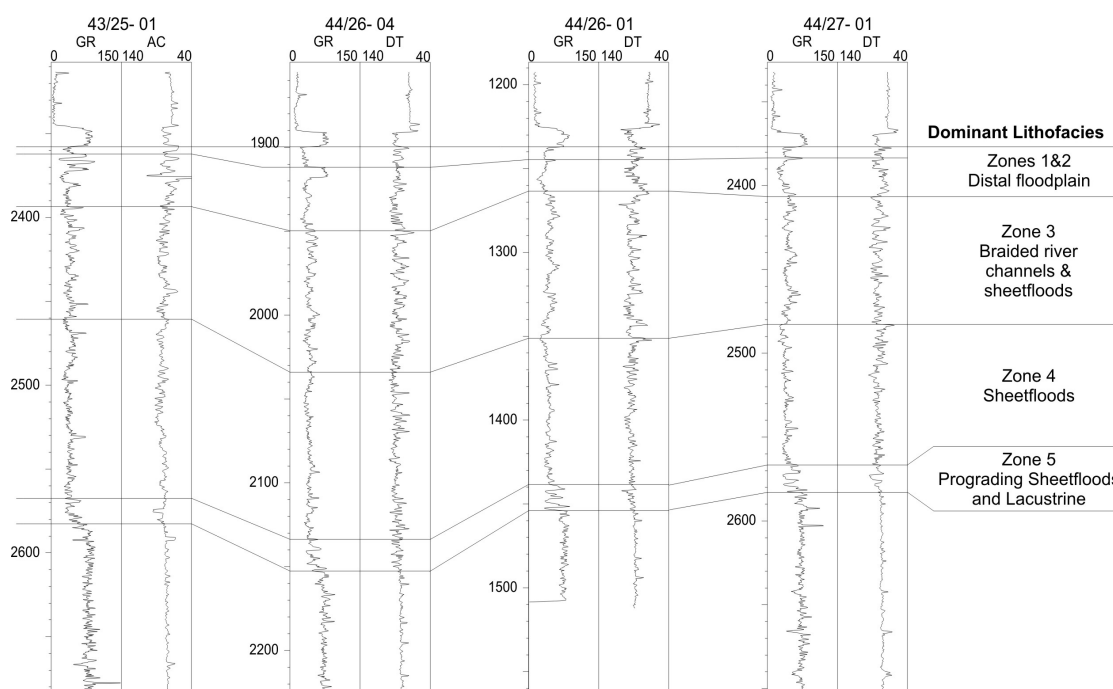
Figure A5.3 Bunter Sandstone Formation well correlation, showing the intra-reservoir zonation and dominant lithofacies. Depths are meters SSTVD.

5.2.1   Petrel-zone 5 Layers

Petrel-zone 5 is the lowermost of the Bunter Sandstone Formation petrel-zones, and is split into two layers which are interpreted to have distinct lithologies; a lower sandstone overlain by shale. This corresponds to zone 7 of Ritchie and Pratsides (1993) for the Caister B gas field.

5.2.2   Petrel-zone 4 Layers

Petrel-zone 4 is the thickest zone and was interpreted to be deposited in a sheetflood environment and is equivalent to zone 6 of Ritchie and Pratsides (1993) for the Caister B gas field. The upper boundary of petrel-zone 4 is marked by a distinct pervasive horizon interpreted to be a cemented sandstone layer. The layering becomes thinner towards the top of the petrel-zone to reflect the increase in alternating shale and sand layers and to preserve the thin cemented layer at the top of the petrel-zone (1 – 2 m thick).

5.2.3   Petrel-zone 3 Layers

The depositional environment of petrel-zone 3 was interpreted as a braided river channel system in which intermittent sheet flood deposits interbedded with thin shales represent deposition outside the channels. 31 proportional layers were added to this zone in order to reflect the channel thickness and the cyclic nature of the sand deposits alternating with thin shales.

5.2.4   Petrel-zone 2 Layers

Petrel-zone 2 represents a distal floodplain setting with minor channels. There is an increase in shale content towards the top of this petrel-zone, along with an increased abundance of

cemented layers relative to petrel-zone 3. This petrel-zone has 10 layers, with the lower 5 layers twice as thick as the upper 5. This reflects the increased abundance of thin shales and cemented layers towards the top of the petrel-zone.

5.2.5   Petrel-zone 1 Layers

Petrel-zone 1 represents a distal flood plain setting with intermittent channels. There is a marked increase in the number of cemented layers observed on the well logs. Proximity to the halite and anhydrite rich sediments of the overlying Haisborough Group may account for the increase in cement-affected sandstones towards the top of the reservoir. Four proportional layers were inserted in order to provide thin layers at the top of the reservoir. This petrel-zone corresponds to zones 1 and 2 of Ritchie and Pratsides (1993).

The resulting model has 57 layers within the reservoir interval with an average thickness of three metres (**Figure A5.4**).
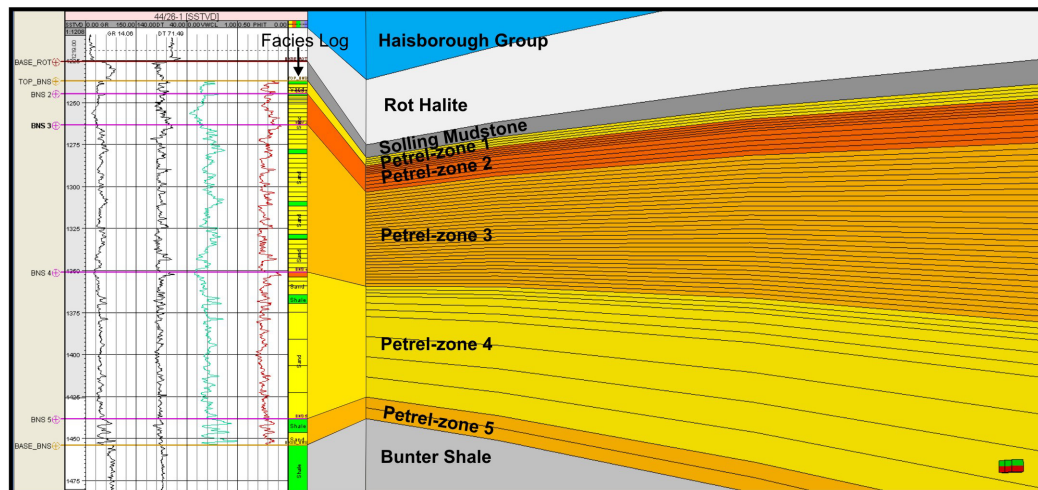
Figure A5.4: Layering and petrel zones in the model and relationship to the facies log

5.3   Bunter Shale Formation Layering

Underlying the reservoir unit a single layer was added to represent the Bunter Shale Formation. This layer forms the underlying seal to the Bunter Sandstone Formation.

5.4   Model Layers and Zones

The final geocelluar model has 9 petrel-zones, 61 layers and a total of 429660 cells assigned with physical properties.

Type	Formation Name	Petrel-zones	Number of Layers	Comments
Upper Seal	Haisborough Group	Haisborough Group	1	
		Rot Halite Member	1	
		Solling Mudstone	2	
Storage Unit	Bunter Sandstone Formation	Petrel-zone 1	4	Cemented sandstones and sandstone. 4 layers to give detail at the top of the storage unit
		Petrel-zone 2	10	Clean sands with shale layer at top of petrel-zone. Thinner layers at the top of the petrel-zone
		Petrel-zone 3	31	Sand alternating shale, even layer distribution in order to capture cyclic nature of this petrel-zone
		Petrel-zone 4	10	Largely clean sand at the base, cemented layer (0 porosity 0 perm) marks the transition into petrel-zone 2. Thinner layering at the top to reflect this
		Petrel-zone 5	2	Thin petrel-zone at base of storage unit. 2 layers: one sand one shale.
Lower Seal	Bunter Shale Formation	Bunter Shale	1	

Total No of layers	61
Total No of cells	429660

Table A5.2: Petrel-zones, layers and cells in the model

6 Well Interpretation, Facies and Property Modelling

Porosity and permeability in the Bunter Sandstone Formation has been complicated by a complex multiphase diagenetic sequence controlled by original texture and by subsequent diagenesis (Bifani 1986). Many of the pore spaces have been filled by cements. For example, halite cement occludes the porosity of sediments that were initially well sorted coarse grained sands in the Esmond complex (Bifani 1986). The relationship of porosity and facies in the Bunter Sandstone will have a major effect on fluid flow and therefore CO_2 injection.

Net to gross and porosity logs were prepared as input for the facies and porosity modelling respectively. 21 wells exist within the model boundaries of which 10 had wireline geophysical logs available over the Bunter Sandstone Formation suitable for petrophysical analysis of lithology and porosity (**Figure A6.1, Table A6.1**). Raw digital log *.LAS files were obtained from the BGS petrophysical log database or IHS for these wells.
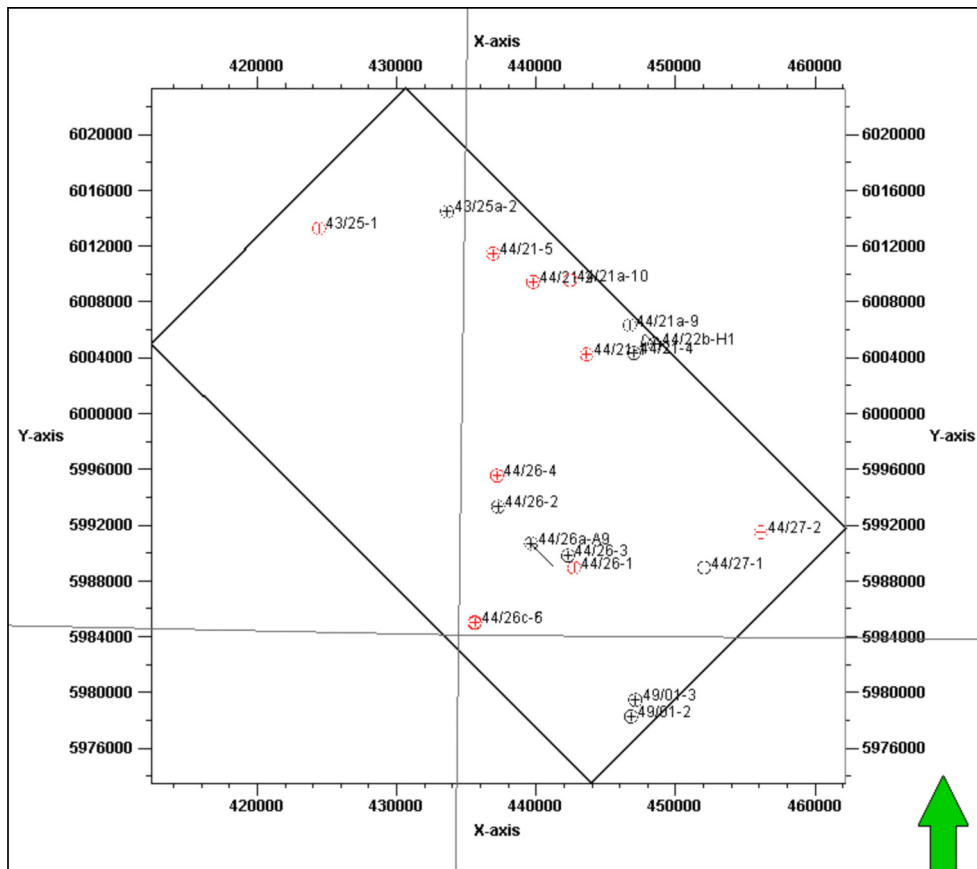
Figure A6.1: Location of wells within the project. red wells are those with wireline logs available from which porosity could be calculated.

Wells with wireline data available	Main log curves available over Bunter Sandstone Formation (BNS) interval	Log quality comments	NTG	Arithmetic mean porosity (PHIT)
43/25-1	Sonic, GR	No LQ curves available	0.906	0.145
44/21-1	Sonic, GR, resistivity	No LQ curves available	0.897	0.158
44/21-2	Sonic, GR, resistivity	No LQ curves available	0.938	0.166
44/21a-10	Density, sonic, GR, resistivity	Large washout in top 5m of BNS. DHRO occasionally spiking >0.1	0.923	0.221
44/26-1	Density, sonic, GR, resistivity	DHRO occasionally spiking >0.1	0.921	0.231
44/26-4	Neutron, density, sonic, GR, resistivity	Possible tool error creating out of tolerance DRHO>0.1 spikes, affecting sections of log	0.966	0.257
44/26c-6	Sonic, GR, resistivity	~5m high washout near the top of the BNS	0.967	0.175
44/27-2	Neutron, density, sonic, GR, resistivity	~15-20m high washout near top of BNS. DRHO>0.1 in that area.	0.914	0.221

Table A6.1: Wells used for petrophysical interpretation

Available well logs include gamma ray (GR), sonic transit time (DT), density (RHOB) and neutron (NPHI) logs among others. Different curves were available for different wells and log data was acquired using tools of varying age, acquired at different times. The method described here was adapted according to well logs and quality of available data. Areas of poor density-neutron log quality were identified and discarded by using the density correction curve (DRHO) and caliper curves (CALI). Assumptions for the log interpretation include a temperature gradient of 35°C/km (with a surface temp of 8°C) where no log metadata was available. Assumptions were also made regarding likely mud type (water based mud assumed), and that suitable environmental corrections were already applied to logs.

6.1   Net to Gross

Net to gross (NTG) for the reservoir was calculated by first generating a volume of shale (V_{sh}) log. Input curves were the GR or density-neutron curves where available. Areas interpreted to represent the cleanest reservoir sand and the most clayey intervals were picked as the end points to create a V_{sh} log scaled from 0 (clean reservoir) to 1 (shale). A reservoir cut-off of 0.6 was then applied, to separate the formation into 'reservoir' (where V_{sh}<0.6) and 'non-reservoir' (where V_{sh}>0.6) to calculate the NTG as follows:

NTG= $\dfrac{\text{Total thickness of Reservoir}}{\text{Total thickness of Reservoir + Non-Reservoir}}$

6.2 Porosity

A total porosity curve was calculated primarily from the density-neutron curves. Areas of poor density-neutron log quality were identified using the DRHO and CALI curves. Over log sections where this was the case, the porosity curve was computed from the sonic log. Some wells had no density-neutron log available and in these instances, the porosity was again computed using the sonic log.

Equations appropriate to the well logs available were used to compute porosity. These take into account tool measurements; shale volume and assumptions about mud filtrate and mud type properties (in the invaded zone surrounding the borehole wall where most of the tools take their measurements), and also rock matrix properties (where these cannot be determined from other tool measurements). The main types of equations used are listed here:

- Sonic (DT) - Wyllie equation

- Density (RHOB) - Standard density porosity equation

- Density-Neutron (RHOB & NPHI) - Standard density-neutron cross plot method

The total porosity curve (PHIT) was provided, to standardise the different measurement types and methods used. Note that this curve generally gives high porosities in shales, which mainly contain very small pores that are largely ineffective. This effect was removed prior to the porosity modelling stages (see section 6.5).

6.3 Lithological Logs

In order to meaningfully simulate the likely behaviour of a reservoir during CO_2 injection, it is important to estimate the property distribution of the static model, based on a facies or lithological model. In this study a combination of deterministic and stochastic lithological distributions were used as a framework for estimating porosity and permeability.

A discrete lithological log was generated for the wells based on the interpreted porosity and V_{sh} curves to use as a base for populating the model with properties. The V_{sh} log was used as the primary discriminator between clean sand (reservoir) and shale (non-reservoir). The V_{sh} cut-off of 0.6 was also used (as per the NTG). Areas of the log which were very clean (V_{sh} close to 0) but had very low porosity (PHIT<0.05) were interpreted to be tightly cemented sandstone. In several cases these could be correlated between wells and were included in the lithological model as a separate discrete lithological description called cemented sandstone. There are three discrete lithology classes present in the model. These are shale, sandstone, and cemented sandstone.

6.4 Facies Modelling

Both diagenesis and the distribution and orientation of facies within the Bunter Sandstone Formation have important implications for fluid flow within the reservoir. Bifani (1986) suggests that before diagenesis, the channel fill had the best reservoir properties, however they have suffered the most pronounced reduction in permeability due to halite cementation. Channel switching and lobe abandonment also added an additional complexity and heterogeneity to the geometry of the sandstone bodies and affect the reservoir continuity (Ketter 1991). This would indicate that flow paths may be quite tortuous and patches of silty

sediments will act as baffles. Flow paths are probably less tortuous in the interpreted mean channel direction (NE-SW). This was taken into account in the facies modelling.

Analysis of the well logs and generation of facies logs within PETREL based on V_{sh} and porosity logs, enabled determination of 3 discrete lithology classes at the well locations to be upscaled into the 3D model grid. These lithology classes were sandstone, cemented sandstone and shale and they were determined from V_{sh} and porosity log cut-offs; (refer to section 6.3). Upscaling of the lithology logs enabled facies modelling to be carried out in each reservoir petrel-zone, honouring the relative proportions and trend distributions of each petrel-zone individually. Facies modelling was achieved by stochastic modelling techniques augmented with strongly deterministic features.

The lowermost petrel-zone 5 has two distinct layers which are laterally continuous (over the entire model area). The layers are based on well interpretation and consist of lower sands and an upper shale dominated unit. As this was correlatable across all of the upscaled lithology logs, kriging was applied with a large range in order to populate the two zones accordingly.

In petrel-zone 4, object modelling was used to ensure channel geometry was reflected in the facies. Channels were interpreted to be several hundred feet wide but only a few feet deep (Ketter 1991) with low sinuosity (Ritchie and Pratsides 1993). In the model the channels were given minimum, mean and maximum widths and thicknesseses in order to capture this. The sediment transport direction is thought to be from the southwest (Ritchie and Pratsides 1993), and this information was used to orientate the channels throughout all the petrel-zones in the Bunter Sandstone Formation. At the top of petrel-zone 4 there is a cemented sandstone horizon which is present in most of the wells in the area, and is regionally consistent with a variable thickness between 1 and 2 m. The cemented layer is locally absent in wells 49/01-03 and 43/22-01. It is thought the location and distribution of this cemented layer may have a major impact on the flow of CO_2 within the reservoir, and therefore was required to be represented as accurately as possible. To ensure this, the cemented horizon was manually 'painted' in. The net to gross in this petrel-zone from well logs is 0.98, indicating that it is a well-cemented clean sandstone.

For petrel-zone 3 the orientation and channel width chosen reflected the channel geometries described in Bifani (1986) and Ketter (1991). Stochastic object modelling was used to add an abundance of sand within a background of shale. The proportions of sand and shale, and vertical distributions were taken from data analysis of the facies logs. The net to gross of petrel-zone 3 in the model is 0.89. The cemented sandstones in petrel-zone 3 were added as elongate elliptical features orientated in the dominant direction of transport.

Petrel-zone 2 has a higher proportion of cemented sandstone and shale than the lower petrel-zones. The orientation of the channels was set to the same values as petrel-zone 3. Again object modelling was used to create sand geometries within a background of shale. This was guided by a trend surface which represents the horizontal proportion of sand and a vertical trend was added honouring the well facies data. The cemented sandstones in petrel-zone 2 were again added as elongate elliptical features orientated in the dominant direction of transport.

In petrel-zone 1 Truncated Gaussian Simulation (TGS) was used to stochastically distribute the sand, cemented sands and shale lithological classes throughout, honouring the likely distribution according to the depositional model and the vertical and horizontal trends

observed from the well data. Analysis of the lithological logs of zone 1 suggests that cemented sandstone and shale do not occur together within any one well. The resultant lithology model for zone 1 therefore exhibits a spatial distribution whereby cemented sandstone and shale rarely occur next to each other; they are separated spatially by areas of clean sandstone. Clean sandstone, cemented sandstone and shale were given elongate variograms trending in the sediment transport direction.
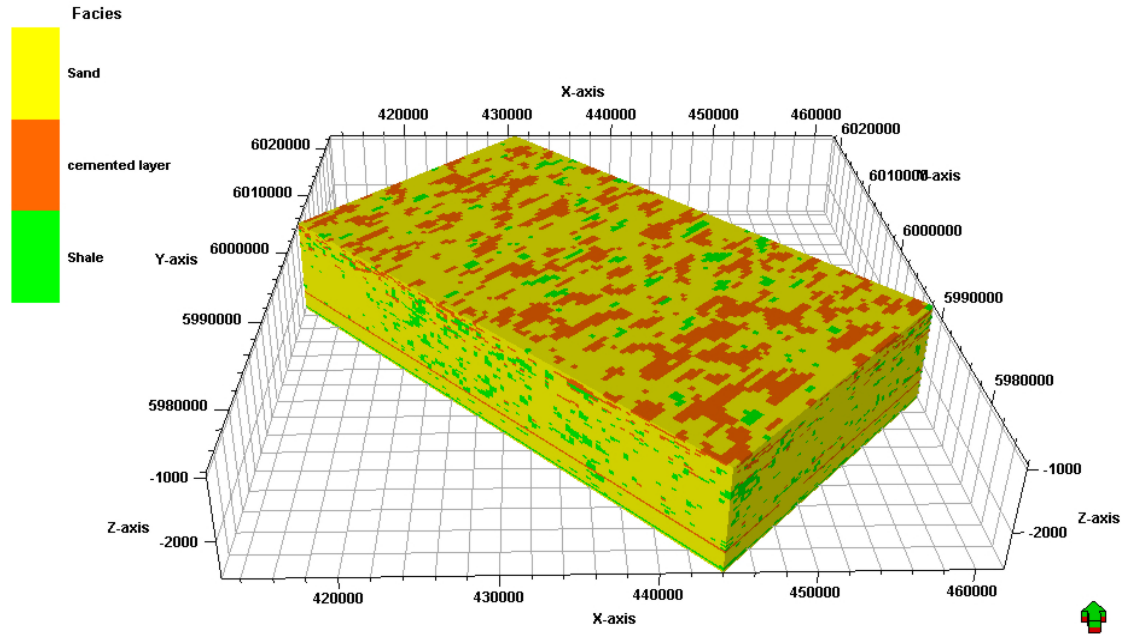
Figure A6.2: Example of the facies in the Bunter Sandstone Formation geocellular model (viewed as regular grid in XYZ)
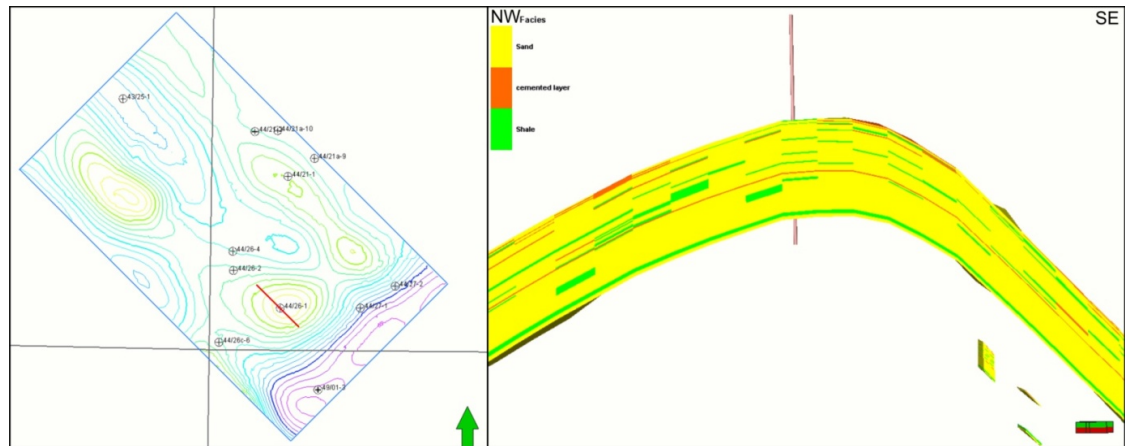
Figure A6.3: Cross section through closure 36 showing facies distribution within the model

With the exception of zone 5 and the upper layer of zone 4 which were populated deterministically, relative proportions of each lithology in all zones were taken from the lithological logs, along with vertical proportions. The resultant stochastic distributions are therefore informed by the trends observed from the upscaled lithology data.

6.5   Porosity and Permeability

Porosity of the sandstone within the Bunter Sandstone Formation was upscaled from the total porosity (PHIT) logs, and distributed within the modelled sandstone lithology using Sequential Gaussian Simulation (SGS). An orientated elongate variogram with a major and minor range of 4000 and 2000 m respectively was used for the stochastic distribution, defined during data analysis. Orientation of the major range was defined in order to distribute porosity along the preferred direction of transport. A vertical variogram of one Meter was given in order to represent the rapid vertical variation in porosity observed in the Bunter Sandstone Formation. The porosity model honors the distribution of porosity observed from the upscaled PHIT logs. The average porosity of the sandstone in the reservoir section of the model is 18%.

As little information is available for the porosity of the mudstones, porosity of the shale lithologies were attributed as constants (2.72 %) taken from an average of porosities given for the Solling Mudstone by Spain and Conrad (1997). This value was also attributed to the Bunter Shale Formation, the Solling Mudstone and the Upper Haisborough Group. Porosity of the Röt Halite Member was assumed to be zero. The cemented sandstones were also assumed to have zero porosity due to total occlusion of the pore space by cements. This assumption is based on the calculated PHIT logs, which exhibit very low porosities, and thus the cemented sands are assumed to have no effective porosity. Lack of physical samples mean that core examination of the cemented horizons is not possible within the model area, however, the cemented layer at the top of petrel-zone 4 can be correlated on sonic and density logs to well 44/23- 01 in the Caister B field. Examination of the core for this well supports the notion that the porosity of the layer is severely occluded by cementation. The porosity and permeability of the cemented sandstones remains a matter of significant uncertainty, and as such should be accounted for during sensitivity analysis of the dynamic modelling results.

Very few permeability data exist within the model area due to the scarcity of core. The permeability values for the sandstone lithology class were taken from a porosity and permeability cross-plot of all Bunter Sandstone Formation core data across the UK sector of the SNS (**Figure A6.4**). The sandstone permeability was populated throughout the grid for Bunter Sandstone Formation reservoir petrel-zones using SGS with a bivariate property distribution linked to the previously modelled porosity grid. A range of possible permeability values could be assigned to each grid cell based on its given porosity value, and the permeability ranges on the cross-plot within a 2% porosity range incorporating the grid cell porosity value. The arithmetic average permeability of the clean sandstone lithology class is 248 mD, with a geometric mean of 10 mD.

All shale lithologies in the model were assigned a permeability of 0.0065 mD, taken from an average of permeabilities given for the Solling Mudstone by Spain and Conrad (1997). This includes the interbedded shales present within the Bunter Sandstone Formation, the Solling Mudstone, the Upper Haisborough Group and the Bunter Shale Formation. The Rot Halite was given a constant porosity and permeability of zero to correspond with its likely properties. As the porosity of the cemented sandstones was assumed to be zero, it was determined that they would likewise exhibit zero permeability. It is stressed that this remains a matter of significant uncertainty, seriously reducing the geometric mean permeability of the model.
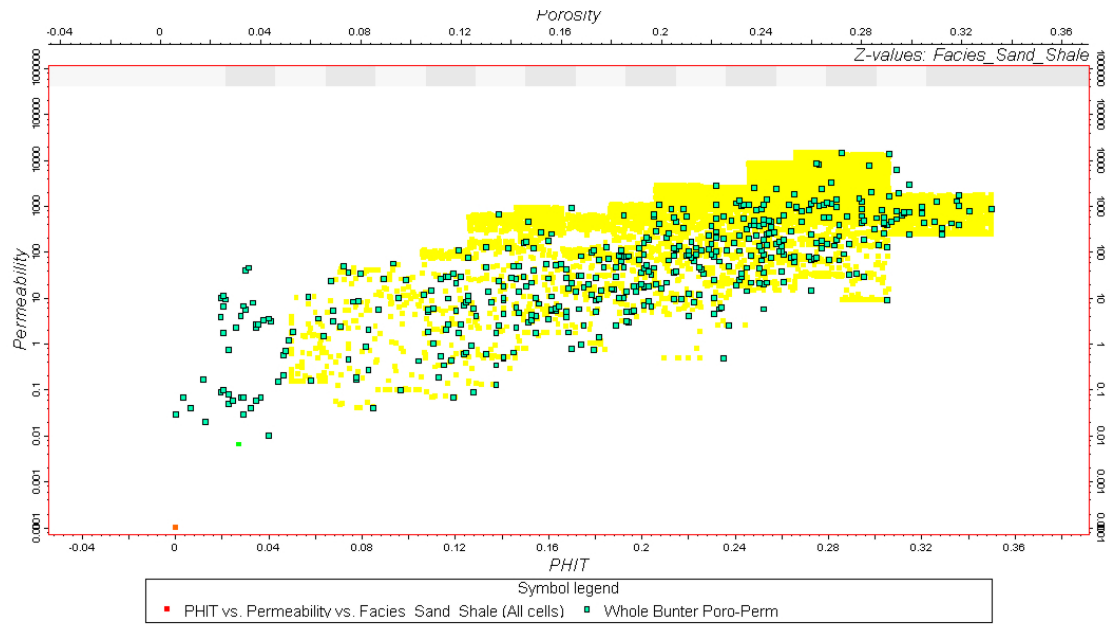
Figure A6.4: Cross plot of porosity and permeability used to guide the permeability distribution in the model. The original core data for the entire Bunter Sandstone Formation are shown by green points. The modelled porosity and permeabilities from the detailed model are coloured by lithology type. Yellow indicates clean sandstone. The red and bright green points represent the constant values given for cemented sandstone and shale respectively

7   Faults

Due to time constraints it was decided that faults would not be incorporated into the model. For completeness and defensibility the presence of faulting was examined in the model area.

An edge map over the model area was received from PGS. The 'Edge' attribute measures the rate of change of dip, and as a result, faults and lineaments are often highlighted clearly (**Figure A7.2**).

The edge map shows no evidence of faulting on the crest of the target dome (closure 36). This assumption was checked by examining an area of 3D seismic data which covers dome 36 for the presence of faulting in the reservoir and immediate overburden. No evidence of large scale faulting was visible on the seismic data provided (**Figure A7.1**). On the crest of closure 36 a possible small fault or fracture is visible, but it is suggested this poses a limited containment risk.
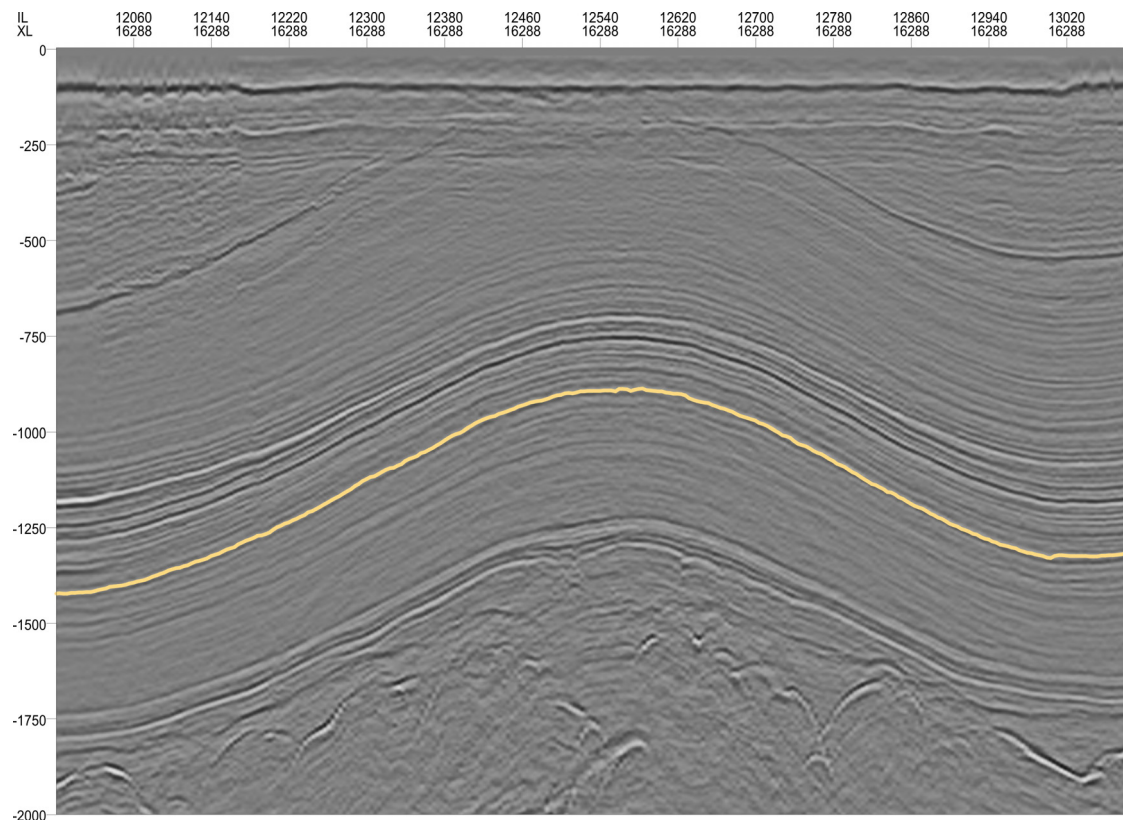
Figure A7.1: Seismic line through closure 36 (line CD on Figure A7.2)
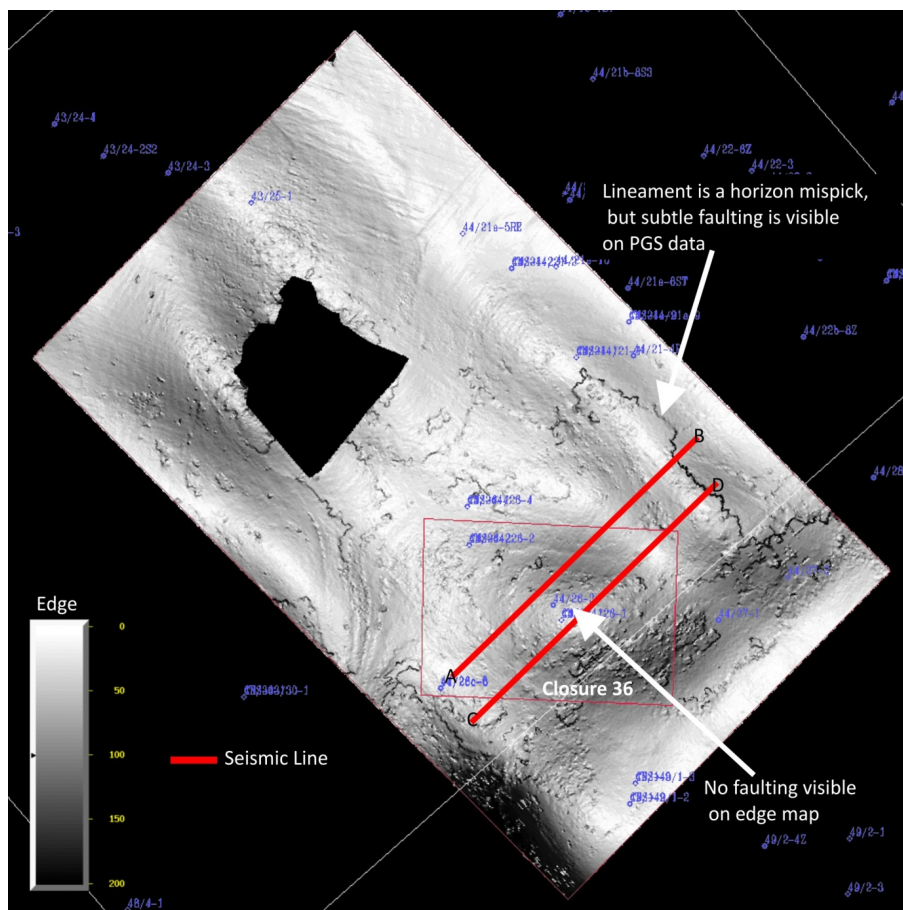
Figure A7.2: Edge map of the top of the Bunter Sandstone Formation horizon pick

The edge map shows a lineament over closure 37. This was interpreted by PGS as a seismic 'mispick' during their interpretation, although some small faulting is observed.

8   Discussion and Summary of Geological Model Build

The porosity and permeability of the shale and cemented sandstones may need further consideration. If the layers are impermeable they may act as barriers to flow for CO_2 and minimise the storage potential of the reservoir or guide the direction in which the CO_2 migrates. Therefore it is important to ensure that the values assigned to these critical layers within the reservoir are correct. Further work may need to be undertaken in order to assess the permeability and porosity of these layers as well as their geomechanical properties.

The thickness of the cap rock overlying closure 36 may also require further validation, especially in the region where it thins in the SE of the model area and directly to the west of the target structure where the reservoir and caprock are uplifted by salt movement (**Figure A4.2**).

Using well logs, core data and seismic surfaces a 3D geocelluar model was created in Petrel of 4 closures in the Bunter Sandstone Formation. Closure 36 was the target feature of later modelling of CO_2 injection. The geocellular model was built with the following considerations:

- Suitable number of cells to allow repeated model runs of CO_2 injection ECLIPSE[TM] simulation software package (Schlumberger, 2010b)

- Retain the major geological and lithological features

Facies interpretation was used to guide reservoir and cap rock zonation and layering. The 3 lithology types within the Bunter Sandstone Formation of sandstone, shale and cemented sandstone were populated throughout the reservoir. Based on well log interpretation the porosity of the sandstone units were populated throughout the model guided by the lithology distribution. Permeability was assigned based on the porosity and permeability values from core data. Constant porosity and permeability values were given to the shales and cemented layers.

9 Data for the Reservoir Simulation Model

The geological model which had been constructed in Petrel, was exported for reservoir simulation using the ECLIPSE 300 simulation package along with the CO2STORE module. Some additional data was required for the simulations.

9.1 Brine Salinity Gradient

As the solubility of CO_2 in brine is reduced significantly with the increase of salinity, for a thick aquifer formation the solubility of CO_2 can be calculated accurately with a gradient of brine salinity in ECLIPSE model. The data is not available from the project database. The following references are used in the Exemplar 2 ECLIPSE model.

The pore space is filled with highly saline salt-saturated water in the southern North Sea, in the absence of halite cement and hydrocarbons. The salinity in the Esmond field is from 13,000 to 205,000 ppm. The viscosity of formation water from Esmond field is about 0.5025 cp with density 1050 kg/m^3 at 1355.75 m. The specific gravity of the brine is approximately 1.21 g/cc at 60 °F (Brook, Shaw et al. 2003).

Smith et al (2010) state that the pore fluid is brine with salinity up to about 300,000 ppm (Smith, Bentham et al. 2010). 130,000 ppm was used by BGS in a project, but it was commented that the brine salinity taken from the paper on the Esmond complex may be too low (130,000 ppm) (Holloway 2010).

The detrital mineralogy of the Bunter Sandstone in the UK sector of the southern North Sea is likely to be similar to that in the Cleethorpes borehole (Lincolnshire), except that some of the porosity is likely to be occluded by halite cement. This is commonly observed in North Sea Bunter Sandstone cores (Brook, Shaw et al. 2003). However, it was decided that there were enough similarities for the lab and field data from Cleethorpes (Downing, Allen et al. 1985) to be used in the model.

The salinity gradient used in the model is 50,000 ppm (0.88 molality) at 1200m and 213,500 ppm (4.65 molality) at 1882m. The depth of the closure 36 is in the range (1200-2000m).

9.2 Pressure, Geothermal Gradients and Compressibility

The Bunter Sandstone formation in the southern North Sea is hydrostatically pressured (Brook, Shaw et al. 2003). The pore pressure gradient used in a previous simulation is 10.67 MPa/km (0.47 psi/ft) (Smith, Bentham et al. 2010); in the CarbonStore database, it is 10.07 MPa/km (0.44 psi/ft) which is calculated from initial pore pressure at the shallowest point and corresponding depth (see **Table A10.3 and Table A10.4** for details). The lithostatic gradient is 22.5 kPa/m (1.0 psi/ft) (Smith, Bentham et al. 2010).

In the absence of any leak-off pressure data, it is assumed, based on an empirical relation between lithostatic (vertical), stress gradient (1.0 psi/ft) and the minimum horizontal stress gradient (0.8 psi/ft), that the leak-off pressure is less than 1.7 x pore pressure (0.8/0.47). Therefore, the pressure increase is less than 0.7 initial pore pressure without considering any safety factor and fracturing pressure gradient.

The geothermal gradient is 36.5 °C/km with temperature = 8 °C at the sea bed based on the CarbonStore database.

Pore compressibility C_p = 5.5675×10^{-4} MPa^{-1}; brine compressibility C_w = 3.1325×10^{-4} MPa^{-1} based on the CarbonStore database taking the average value from Closure 36 to Closure 38.

9.3   Relative Permeability and Capillary Pressure

Four types of relative permeability and capillary pressure curves are recommended by RPS (see Appendix A5.1) to use for permeability values from 0.1mD to >100mD as shown in **Table A9.1**. Two new properties SATNUM and IMBNUM were set up in the Petrel model as properties based on permeability ranges and exported to the ECLIPSE model so that the code would know which relative permeability curve to use in a simulation. There is no imbibition data available for Viking_I and Berea samples. Also, there is a lack of evidence to prove that Berea curve, which has a very high relative permeability to CO_2, is suitable. These two curves were therefore not used in the Exemplar 2 model. The Calmar curve is used for shale and caprock and the Viking_II curve is used for sandstone. The two relative permeability curves are shown in **Figure A9.1**.

Most of properties used in the ECLIPSE Exemplar 2 model are listed in **Table A9.2**, along with references. The table also shows some data from other references, which were not used in this model, but were used in other work.

Formation	Permeability Range (mD)	Measured imbibition data available	Used in Exemplar_2 model
Calmar	k<0.1 mD (shale, caprock)	Yes	Yes
Viking_I	0.1 mD < k < 10 mD	No	No
Viking_II	10 mD< k < 100 mD	Yes	Yes
Berea (Stanford)	k> 100 mD	No	No

Table A9.1 Relative permeability and capillary pressure recommendations
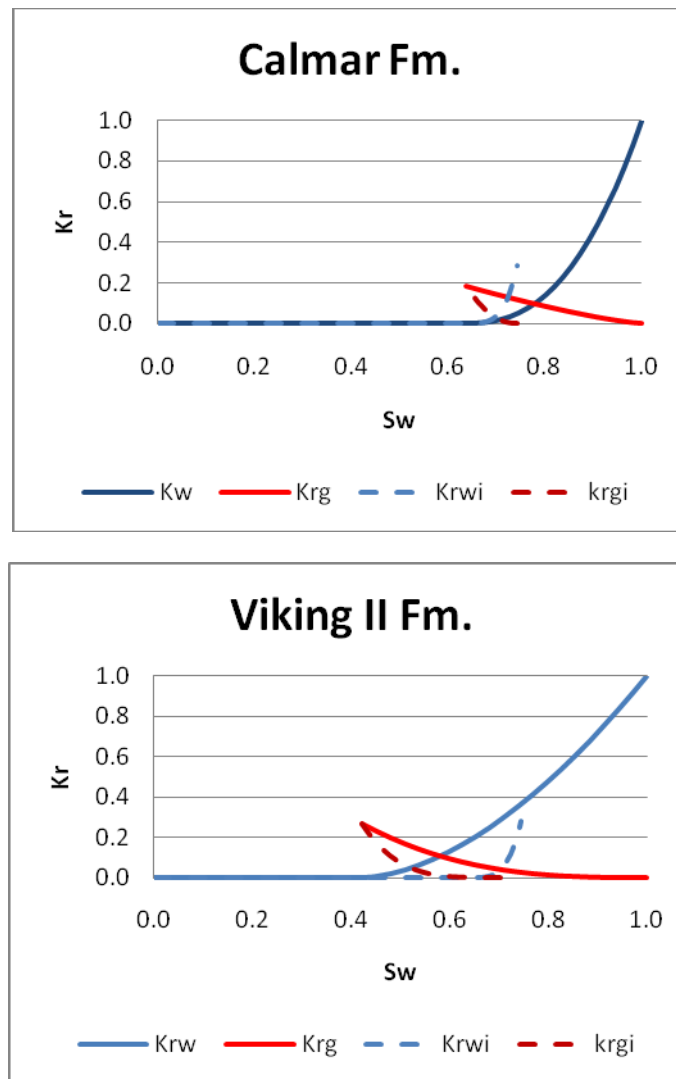
Figure A9.1: Relative permeability curves used in the ECLIPSE Bunter model; top – for shale and caprock, bottom – for Bunter sandstone

Parameters	unit	value	reference
Rock compressibility	1/MPa	5.5675×10^{-4}	www.carbonstore.org.uk average of Closure 36, 37, 38, 39
Water compressibility	1/MPa	3.1325×10^{-4}	www.carbonstore.org.uk average of Closure 36, 37, 38, 39
Brine salinity and gradient	ppm	180,000 130,000-205,000 50,000-200,000*	www.carbonstore.org.uk (Brook, Shaw et al. 2003), Holloway, 2010 CASSEM Lincs data (Downing, Allen et al. 1985)
Brine viscosity	cp	0.3	Default in ECLIPSE E300, but will recalculated from PVT
Temperature gradient	C/km	36.5* 35.0	www.carbonstore.org.uk Smith et al, 2010
Sea bed temperature	C	8* 4	www.carbonstore.org.uk Smith et al, 2010
Pressure gradient	MPa/km	10.07* 10.67	www.carbonstore.org.uk Smith et al, 2010
Lithostatic pressure	MPa/km	22.5	Smith et al, 2010
Fracture pressure/initial pressure		1.4	P(inj max) = 0.8 Lithostatic pressure x 0.9
Average porosity in boundary aquifers		0.2	www.carbonstore.org.uk Smith et al, 2010
Average permeability in boundary aquifers	mD	100	www.carbonstore.org.uk Smith et al, 2010
Rel perm curves		2 Drain + 2 Imb**	Appendix A5.1
Boundary condition		PV=280 km^3 for Zone 4, vary with models	www.carbonstore.org.uk
Total field injection rate	MT/yr	10~20	Holloway, 2010

* value used in ECLIPSE model
** Drain – drainage curve, Imb – imbibition curve.

Table A9.2: Properties used in Exemplar 2 (Bunter) model

10 Static Capacity Estimates

A review of static capacity estimates was carried out prior to making dynamic capacity estimates. These estimates combined previous work in the Bunter Formation with data from Carbonstore. The static capacity estimates were used as a guide when deciding on the number of wells and the injection rates in the dynamic models.

The definition of pore volume utilisation (E) is the ratio of the volume of injected CO_2 to the total pore volume of the storage region, which could be a basin, part of a closed formation, or a dome. In order to distinguish the coefficient for a field/basin from the coefficient for a dome/closure, in this study the latter is called local coefficient (E_d). For a closed system, the coefficient is often less than 1%. However, for an open system the coefficient can be as high as 40%~65% depending on the boundary conditions, relative permeability, etc (Brook, Shaw et al. 2003). The static estimation of Bunter formation storage capacity has been made in several projects previously at different scales. Some results are presented below.

10.1 Storage Capacity for a Closure

It is assumed that each closure has an open boundary. The volume of a closure can be calculated by using seismic reflection data and a digitised map. In this project the volume was calculated by Petrel using surfaces with a spill point plane. The storage capacity for each closed structure (dome) was calculated in tonnes of CO_2 using the equation below, and assuming a PV utilisation of 40%, i.e. an average gas saturation of 40 vol.-% (Chadwick, Arts, et al., 2009). The results are listed in **Table A10.1**.

mass of CO_2 tonnes = {area x thickness x porosity x density of CO_2} x PV utilisation

$$= \text{pore volume x density of } CO_2 \text{ x PV utilisation} \qquad (10\text{-}1)$$

Storage_Unit_ID	Storage_Unit	Shallowest Depth (min) = depth to crest of closure	Area (km^2)	TVT_thickness_mean	Porosity ML	PV (m^3)	CO$_2$ density (kg/m^3)	pore volume utilisation (%)	CO$_2$ stored (MT)
139.016	Closure 36	1211.0	71.1	221	0.15	2.12E+09	847.5	40	719.93
139.017	Closure 37	1403.3	86.9	212	0.15	2.58E+09	781.9	40	805.60
139.018	Closure 38	1605.2	32.6	195	0.22	1.22E+09	784.5	40	383.16
139.019	Closure 39	1172.1	73.3	251	0.14	2.32E+09	738.6	40	685.32

Table A10.1: Static estimation of closure storage capacity (assuming PV utilisation E=40%), taken from CarbonStore

10.2 Storage Capacity for Zone 4

Two methods were used to estimate the storage capacity for the Bunter Sandstone formation Zone 4. The first one takes Zone 4 as a closed system, so the capacity depends on the allowable pressure increase and compressibility of the pore spare and water. On the contrary, the second one takes Zone 4 as an open system. The capacity is the sum of the capacity of

each closure, which depends on the spill point, the sweep efficiency and the pressure at the shallowest depth.

For a closed system, the capacity was calculated using the equation below.

$$\text{Mass of } CO_2 \text{ tonnes} = (C_p + C_w) \times \Delta P \times \rho_{CO2} \times PV \tag{10-2}$$

where C_p and C_w is the compressibility (in units of 1/MPa) of the pore space and water, respectively. ΔP is the allowable field average pressure increase (MPa), PV is total pore volume (km^3), and ρ_{CO2} is the average density of CO_2 (t/km^3).

If the density is assumed to be 700 Mt/km^3, ΔP=5 MPa (note that this is an increase in field average pressure), the total PV = 280 km^3 for Zone 4, and the total compressibility ($C_p + C_w$) = 8.7×10^{-4} 1/MPa (from **Table A9.2**), then the capacity is:

$$\text{Mass of } CO_2 = 8.7 \times 10^{-4} \times 5 \times 700 \times 280 = 852.6 \text{ Mt.}$$

Calculation of the Pore Volume Utilisation

Before running a dynamic simulation, the pore volume utilisation from previous studies for the Bunter Formation was reviewed. The main references are from the GESTCO project report (Brook, Shaw et al. 2003) and published papers (Smith, Bentham et al. 2010). A summary is given in **Table A10.2**.

Exemplar Esmond model (one closure model)

Brook et al (2003) described a study in which the Esmond field was assumed to be a virgin aquifer. They estimated that the volume of CO_2 which can be injected into the Esmond gas field is 65% of the pore volume, assuming an open aquifer. They also estimated that the capacity assuming a closed aquifer is 3.5 Mt. As the total pore volume of the Esmond model was not given in the report, it was deduced using Eq. 10-1. If 31.6 Mt of CO_2 is injected, and the CO_2 density is 641 kg/m^3, the total pore volume of Esmond gas field is approximately 7.6×10^7 m^3. The pore volume utilisation (E) for the closed aquifer model may be estimated from the ratio of the capacity of the closed aquifer to the capacity of the open aquifer, assuming that the pore volume utilisation remains constant. The pore volume utilisation of the closed aquifer is 7.2% (= 65%x3.5/31.6). The PV utilisation of a closure (E_d) is between 7.2% and 65%.

Whole Bunter Fm model (multi-closure model)

From static estimates in the Bunter Formation, Smith et al. (Smith, Bentham et al. 2010) calculated that the capacity is 2200 Mt for a closed aquifer, and 4400 Mt for an open aquifer with structural closures, assuming that the domes make up 2% of the pore volume and that the dome PV utilisation is 40%. The total pore volume of Smith's model can be calculated from Equation 10-1, assuming that the density of CO_2 is 800 Mt/km^3, as 343.75 km^3 (350 km^3 in Smith's report). The total volume of injected CO_2 is 2200Mt/800Mt/km^3=2.75km^3. The PV utilisation of the calculated Bunter Fm is between 0.7% and 1.4%.

Then, 10 closures (with no faults) were chosen (Williams and Bentham 2011) with a total pore volume of 19.8km^3 based on the data from the CarbonStore database. Therefore in our case, the PV of the domes is 5.8% of the total PV. The PV utilisation E for whole Bunter Fm model is then:

E = total volume of injected CO_2 in 10 closures / total PV of Bunter Fm

= 19.8 km^3 x 0.4 / 343.75 = 2.3%,

assuming that the local storage efficiency for a dome is 40%.

Actually, the Bunter Fm is assumed to be open here, i.e. the formation consists of closures in an open parent formation. Otherwise, the coefficient is too high for a closed system. In other words, the 40% local pore volume utilisation for each closure may not be reached if the parent system is closed. Generally, if the volume of closures is 2% of volume of the parent (here the parents are Zone 4, Zone 5 and part of Zone 6), and the coefficient of each closure is 40%, the coefficient of the parent is 2%x40% = 0.8%. It does not matter whether the parent is a closed system or an open one with closures, the coefficient is reasonable. For a closed system, the allowable average pressure increase can be calculated using Equation 10-2. Taking the values used above (i.e. mass of CO_2 injected = 2200 Mt, density = 800 Mt/km^3, and PV = 343.75 km^3) and assuming that the total compressibility is 10×10^{-4} 1/MPa, then the allowable pressure increase is 8 MPa. If the initial pore pressure is 20 MPa, and we assume that the allowable maximum pressure is 1.4 x pore pressure, the maximum pressure will be 28 MPa. In other words, the reservoir has to be deep (>2000m). For Bunter Formation Zone 4, the average depth is 1300m. It is hard to get a coefficient of 0.8% if the system is closed.

Region	Open	Closed
Esmond Field	65%	7%
Single Dome	40%	
Bunter (2% of PV in closures)	0.8%	
Bunter (5.8% of PV in closures)	2.3%	

Table A10.2: Summary of pore volume utilisations from static estimates

Storage_Unit_ID	Storage_Unit	Shallowest Depth (min) = depth to crest of closure	Depth to centroid of Storage Unit (m TVDSS)	Closure_Height_(total_relief)	Area (km2)	TVT_thickness_mean	Rugosity of top surface	ShortAxis_Length	LongAxis_Length	Av. Area Net Sand	Av. Vertical NTG	Porosity ML	Permeability (mD)	Faulted	Offset greater than caprock	GRV (x10^9 m3)	PV (x10^9 m3)
139.016	Closure 36	1210.98	1568.78	494.56	71.1	221.03	2.238	7287	12375	0.99	0.91	0.15	50	No	NA	15.7	2.12
139.017	Closure 37	1403.25	1660.17	301.49	86.9	212.34	1.420	5570	21320	0.99	0.94	0.15	50	Yes	No	18.5	2.58
139.018	Closure 38	1605.19	1751.12	96.43	32.6	195.42	0.493	4092	11515	0.99	0.88	0.22	100	No	NA	6.37	1.22
139.019	Closure 39	1172.09	1566.64	538.19	73.3	250.91	2.145	6338	14522	0.99	0.91	0.14	100	No	NA	18.4	2.32

Table A10.3: General data from UK SAP database

Storage_Unit_ID	water compressibility (1/Mpa)	pore compressibility (1/Mpa)	Temperature gradient (c/km)	Temperature at Centroid (C)	Pore pressure gradient (MP/km)	Pressure at shallow end	Pp init (Mpa)	Lithostatic Pr (Mpa)	Fracture pr(Mpa)	pressure incr Mpa)	CO_2 density (T/m3)	pore volume utilisation (%)	CO_2 stored (MT)
Closure 36	0.000313	0.000498	36.65	65.5	10.07	12.2	24.5	21.4	7.06	0.8475	0.597	10.74	
Closure 37	0.000307	0.000601	36.43	68.5	10.05	14.1	29.0	29.0	11.92	0.7819	1.087	21.80	
Closure 38	0.000321	0.000508	36.24	71.5	10.09	16.2	34.4	32.0	12.64	0.7845	1.048	10.04	
Closure 39	0.000312	0.000620	36.70	65.5	10.07	11.8	24.9	21.7	7.92	0.7386	0.7388	12.65	

Table A10.4: Storage capacity calculation (static method)

11   Model Set-up

Before running the simulations to determine the storage capacity and to perform sensitivity studies, a number of decisions had to be taken regarding the well locations, injection rates and well controls. These are described in the following sections.

11.1   Injectivity

Vertical wells were used in all of the case study models, and all of the sandstone layers were perforated, i.e. from layer 8 to layer 62 (i.e. through Petrel zones 1 – 4). The diameter of tubing was 7 inches. The well locations were chosen randomly along a depth contour (e.g. at a depth of 1300m, 1450m, or 1600m), without taking account of the permeability distribution.

From Sections 10.1 and 10.2, the estimated storage capacity for a closure in the Bunter Fm is about 800Mt. If a 50-year of life span for a power station is assumed, with an emission of 8-10 Mt/yr CO_2 (ballpark emissions from 2 a GW coal-fired power plant), 10 wells in each closure are required for a reservoir with moderate injectivity in order to maintain a constant injection rate for 50 years. Several injection scenarios were tested, injecting into one, two or three domes, with 10 wells in each dome.

From the ECLIPSE output, the connectivity parameter kh value (permeability x thickness mD-m) of all 30 injectors in 3 closures is between 14300 and 132600 mD-m. The thickness of sandstone is about 190m in Closure 36 and Closure 39, and 230m in Closure 37, which shows an average permeability between 75mD and 690 mD.

As discussed in Section 9.2, the allowable bottom hole pressure (BHP) was set to be 0.9 x fracturing pressure, and it was assumed that the fracturing pressure was 0.018 MPa/m (0.8 psi/ft). Taking Closure 36 as an example, the initial pore pressure at the shallowest point (crest) is 128 bars at 1211m, the maximum allowable bottom pressure at that depth is 200 bars.

The wells in each closure were grouped. One additional pressure monitoring well was placed on the crest of each closure. For the storage capacity estimation, the maximum injection rate for each well was set initially to 2 Mt/yr. Each injector was controlled by a maximum BHP that was calculated based on the depth at which the injector was perforated, and by the pressure of the monitoring well. If the BHP in any wells exceeded the maximum allowable pressure for that well, the injection rate of the well was reduced. If the BHP of monitoring well exceeded its maximum allowable pressure, the injection rate for each injector in that closure was reduced by 20%.

The above calculation for injection rate and number of wells was based on the permeability data available from the CarbonStore database at the time the model was built. The permeability values were based on the core plug data from the Esmond, Forbes, Gorden, Orwell and Hewett fields (average permeability = 100mD). If these values were overestimated, as suggested by some researchers, then more injectors might be required.

11.2   Closure Pore Volume and Inter-region Mass Flow Calculation

Using Petrel, an intersection plane was made as shown in **Figure A11.1**. Moving the plane up and down, the intersection with the top surface of Bunter Sandstone could be located and the depth of the spill point determined. Once the depth of the spill point was found, the volume between top and bottom of Bunter Sandstone (excluding Petrel zone 5) was calculated for each closure. Note that the depth for each closure was different in different injection scenarios, as shown in **Figure A11.1**. If only Closure 36 was used to store CO_2, the spill depth was 1730m (top diagram). If Closures 36 and 37 were both used to store CO_2, the spill depth was 1760 (lower diagram). The calculation of local pore volume utilisation (E_d) uses the corresponding pore volume to calculate the coefficient, i.e. PV(C36)/PV(total) or PV(C36+C37)/PV(total), as shown in **Figure A11.2**.
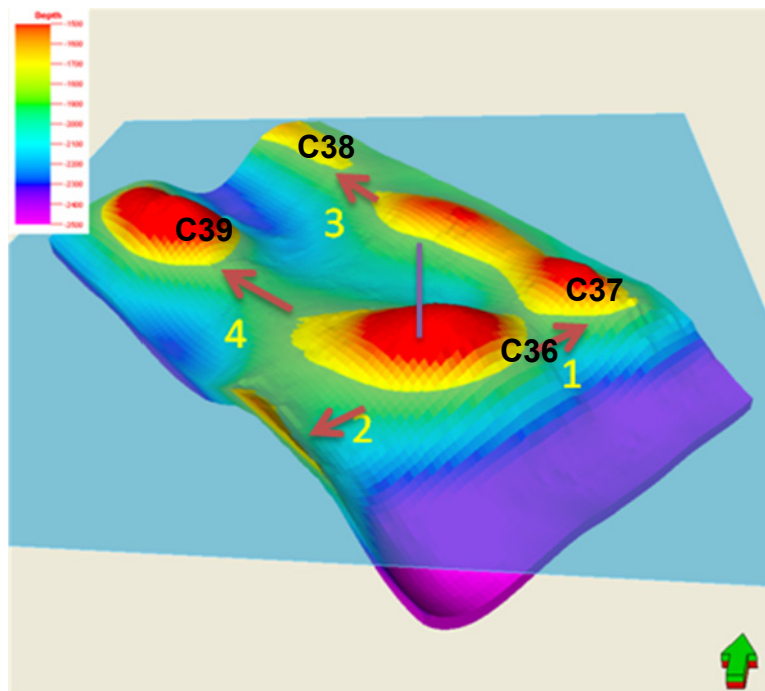
Spill depth = 1730m from C36 to C37, 1760m from C36 to salt wall at the South West, 1785m from C37 to C38, 1855m from C36 to C39
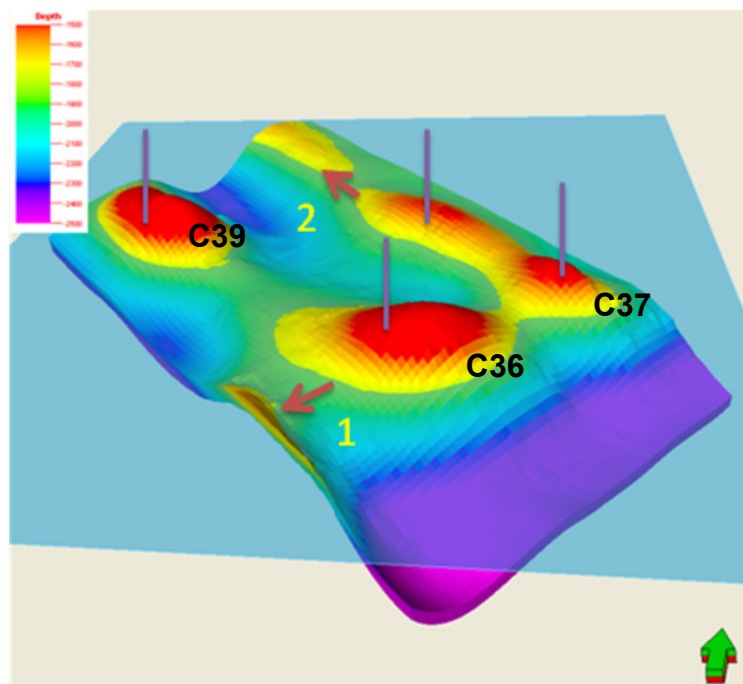
Spill depth = 1760m from C36 to the salt wall at the South West for injection in both C36 and C37, and 1785m from C37 to C38

Figure A11.1: Pore volume and spill depth of a closure
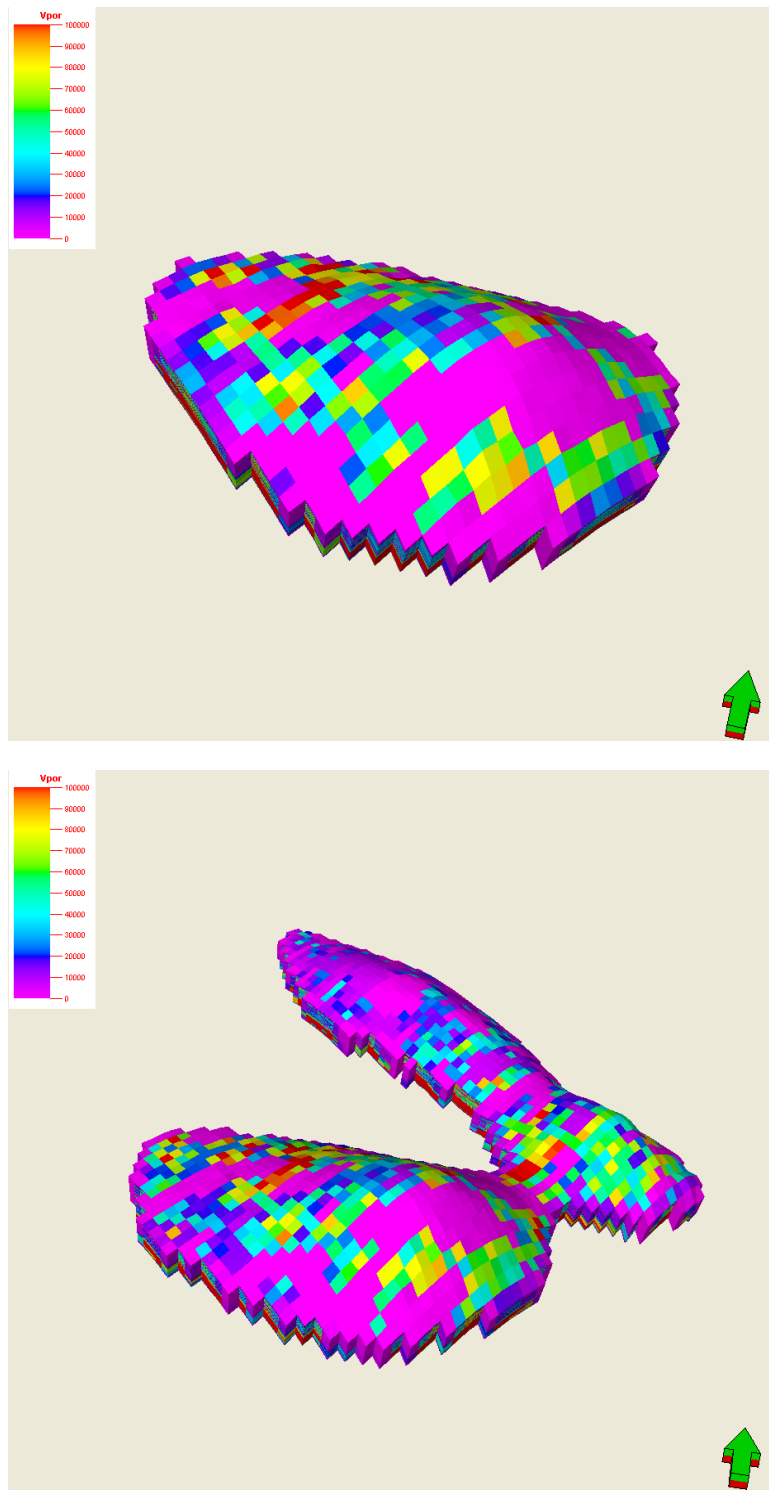
Figure A11.2 Pore volume for Closure 36 (top) and Closure (36+37)

The model was divided into several regions based on the location of the spill points, as shown in Figure A11.3. The ECLIPSE simulation output the cross region flow rate and the total amount of CO_2 vs. time. A criterion was set to measure the spillage. The limit for the ratio of the total mass of spilled CO_2 to injected CO_2 was set to 0.01%. The effective injection time was the date when this criterion was reached. The capacity for this closure was the volume of injected CO_2 at that time.

Figure A11.3 shows how the model was split up into regions to calculate the spillage from different domes. The regions at the outer boundary in Figure A11.3 show the numerical aquifers which represented the extended volumes from the model. Displaced water with dissolved CO_2 and free CO_2 (in the supercritical phase) were allowed to flow into the regions. If the injected CO_2 flowed out of a dome region, the total amount was calculated to compare with the criterion. In different injection scenarios, the calculation of the total inter-regional flow was different, as shown in Table A11.1. If CO_2 was injected into Closure 36 only, the inter-region flow from R16 to R17 was taken as spillage. However, if CO_2 was injected into both Closure 36 and Closure 37, the inter-region flow between R16 and R17 did not count as spillage. In this case, the crosses in Table A11.1 indicate which regions represent spillage.

In multi-dome injection scenarios, injectors were divided into groups. The spillage of each closure was calculated separately. Once the spillage from one closure exceeded the criterion, all the wells in the closure were shut, but the injection into other closures continued.
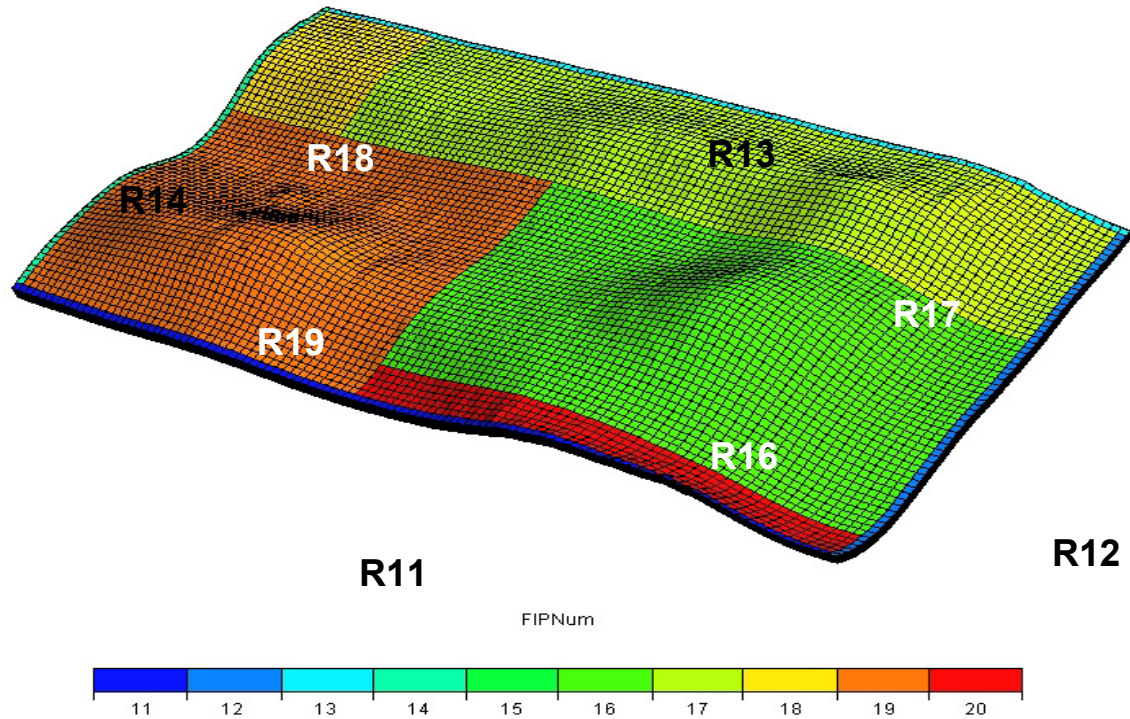
Figure A11.3: Regions shown in different colours for the calculating the spillage of CO_2 from one Closure to another or flowing out of the model

closure	R16-20	R16-12	R16-17	R16-19	R17-12	R17-13	R17-18	R19-11	R19-14
C36	X	X	X	X					
C36+C37	X	X		X	X	X	X		
C36+C39	X	X	X	X				X	X
C36+C37+C39	X	X		X	X	X	X	X	X

Table A11.1: Cumulative inter-regional flow for different injection scenarios in the calculation of filling ratio (spilling ratio), (a box marked "x" indicates where spillage may occur due to flow from one region to another.)

11.3   Well Location and its Impact on Closure Storage Capacity

The location of a well relative to the crest or a spill point is very important for structural trapping of CO_2. As shown in **Figure A11.4**, wells were located along contour of depths of 1300m, 1450m, or 1600m in three cases in order to optimize the base case. In another case, the injectors were all at the crest, even though this is not the best one from injection and storage point of view as:

- the pressure at the crest will increase very quickly because of local pressure build up; the crest may be the weakest part with the risk of fracturing;

- if more wells are drilled on the crest, the potential for future spillage may be increased;

- If the wells are controlled by the pressure at the crest, the injection rate will be reduced in the early stages of injection so that the total injection rate will be restricted and a longer time (hundreds of years) will be required to fill the closure;
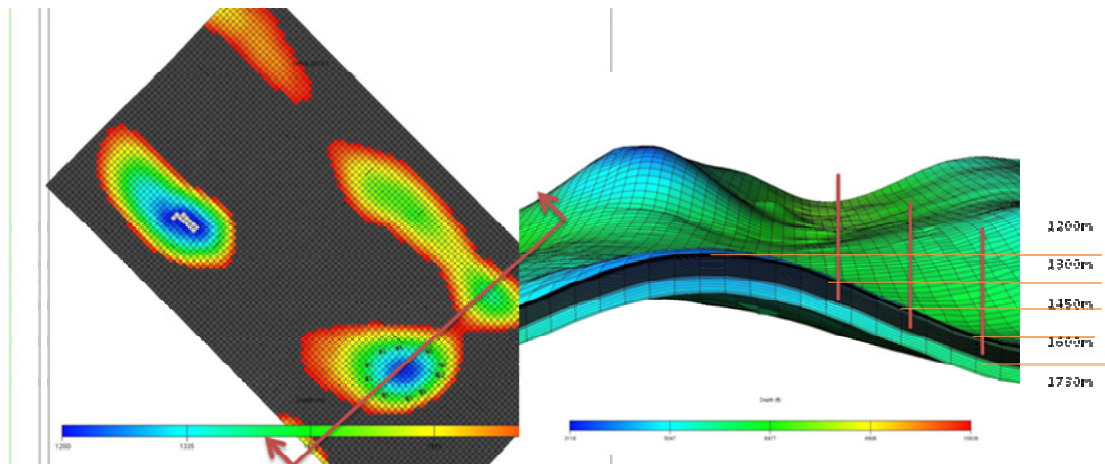
Depth contour and well locations

Figure A11.4: Cross section view (right) of Bunter sandstone with well locations on a depth contour map (left). The colour shows depths between 1200 and 1750m; the depth of the crest is 1200m and the spill point is at 1730m. The depth of the first perforation is set to 1300m, 1450m, and 1600m in three cases
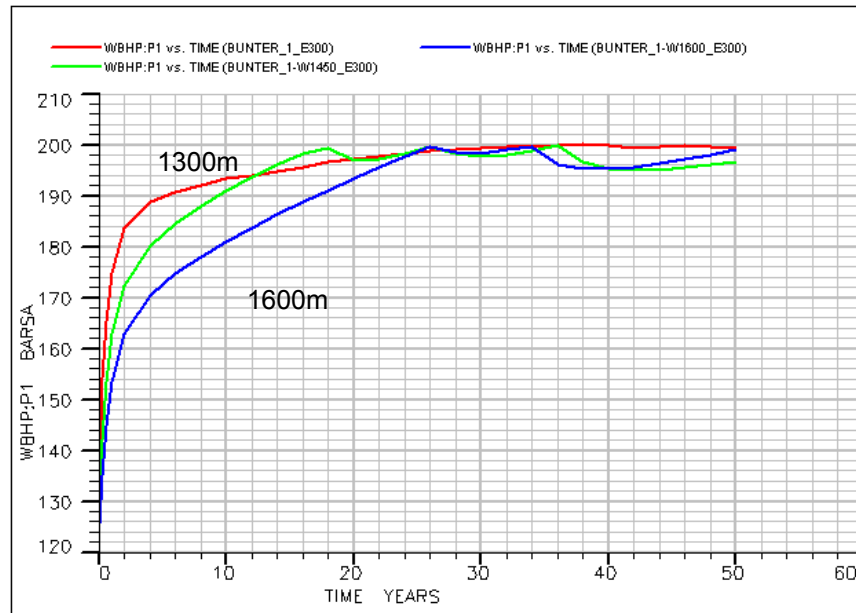
Figure A11.5: The bottom hole pressure (BHP) of the monitoring well, which is at the crest of Closure 36, for injectors at 1300m (base case), 1450m, and 1600m; the spill point is at 1730m
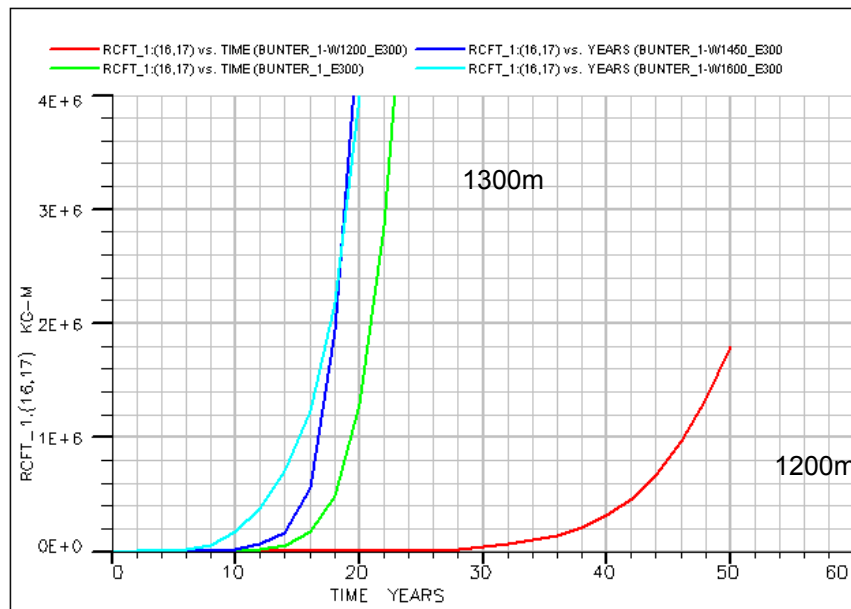
Figure A11.6: The total inter-region flow mass (RCFT) in kg-mole vs. time for 4 different well location scenarios.

Figure A11.5 shows the bottom hole pressure of monitoring well P1 vs. time from three different well-location cases. Because the wells were controlled by both the BHP of each individual well and the BHP of the monitoring well, once the pressure exceeded the fracturing pressure at the crest point, the injection rate for each well was reduced by 20% in the simulation. The simulation results also show that even if the BHP in each injector is capped by its maximum allowable pressure, the pressure at the shallowest point may still exceed maximum allowable pressure. The monitoring well control started at about 18 years for the 1450 m case (green line), and at

about 25 year for the 1600 m case (blue line). It is also shown that when the injectors are further from the crest, it takes longer for pressure at the crest to increase. Therefore, a higher injection rate can be maintained. However, the further the well is from the crest, the closer it is to the spill point, and the sooner injected CO_2 reaches to the spill point.

Figure A11.6 shows the total inter-region mass flow vs. time. The times for the spillage ratio to reach the criterion in the 1600m, 1450m, 1300m, and 1200m cases are: 12, 16, 20, and 46 years, respectively. There is an optimum location (distance from the crest) for the wells, so that there pressure in the crest does not reach a maximum too quickly, but the CO_2 does not reach the spill point early.

11.4 Pressure Response in Neighbouring Closures

Figure A11.7 shows the pressure build up due to the injection of CO_2 into Closure 36. It can be seen that the pressure in Closure 37 also increases due to the injection in Closure 36. This means that the capacity of Closure 37 is affected by the injection nearby. Taking Zone 4 as a whole closed system, if CO_2 is injected into Closures A, B, and D sequentially, the pressure restriction for the capacity of each dome depends on the difference between the local allowable crest pressure and current pressure. The pressure at the shallowest point (crest of Closure 36, in this case) can also increase due to the injection in the neighbour closures. To avoid post-injection failure, the injectors in multi-dome scenarios were also controlled by the pressure at the shallowest point.

Figure A11.8 shows the pressure at the crest of Closure 36 (point A in **Figure A11.7** – red), 37 (B – dark blue, C-green), and 39 (D – light blue) vs. time for the base case (Zone 4 closed), model closed (middle), and open cases (bottom). Because the injectors are controlled by crest pressure in Closure 36, the pressure (red line) in each case is capped at 200 bars. The pressure in Closures 37 and 39 in the open case increases at the beginning of injection, and then stays constant. On the contrary, the pressure of other domes (where no injection is occurring) in the closed case increases much more quickly. The closer a dome is to an injection dome, the larger the pressure increase. The preliminary simulations described in this Chapter, allowed us to choose a base case model for the capacity estimates. This was the model with the wells at 1300 m.
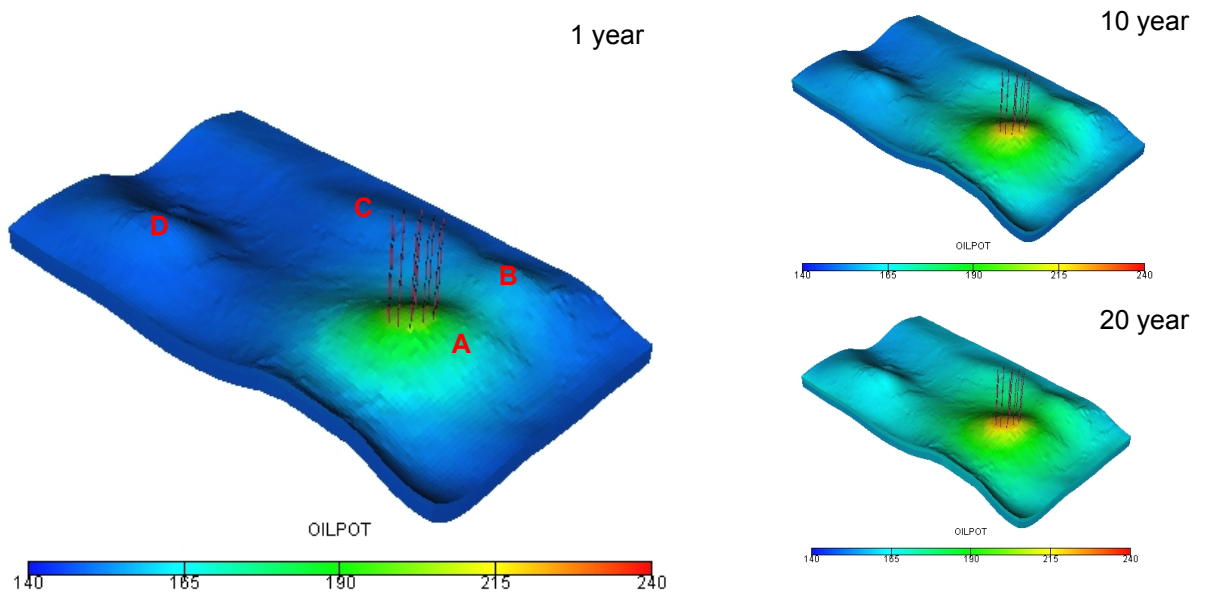
Figure A11.7: The pressure increase (build up) after 1, 10, and 20 years injection in the base case.
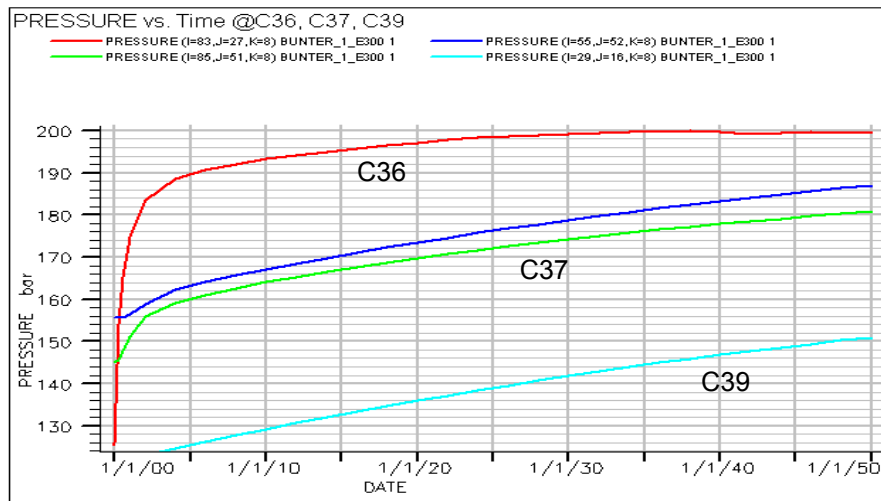
(a) base-case
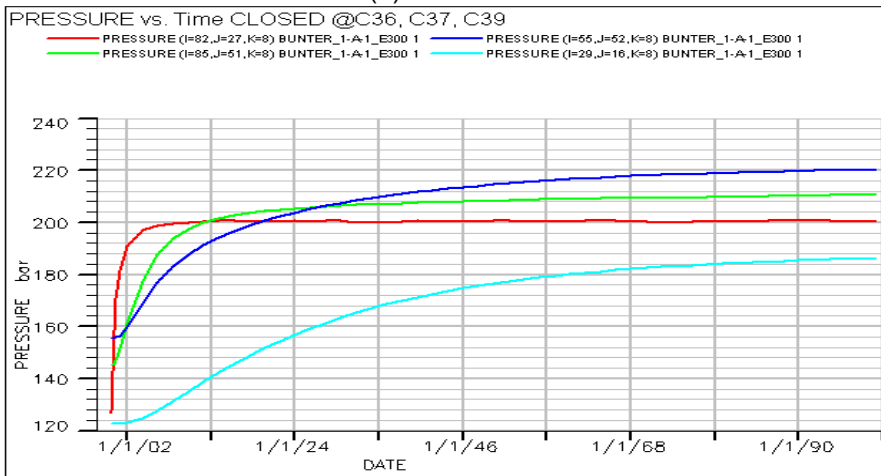
(b) closed boundary
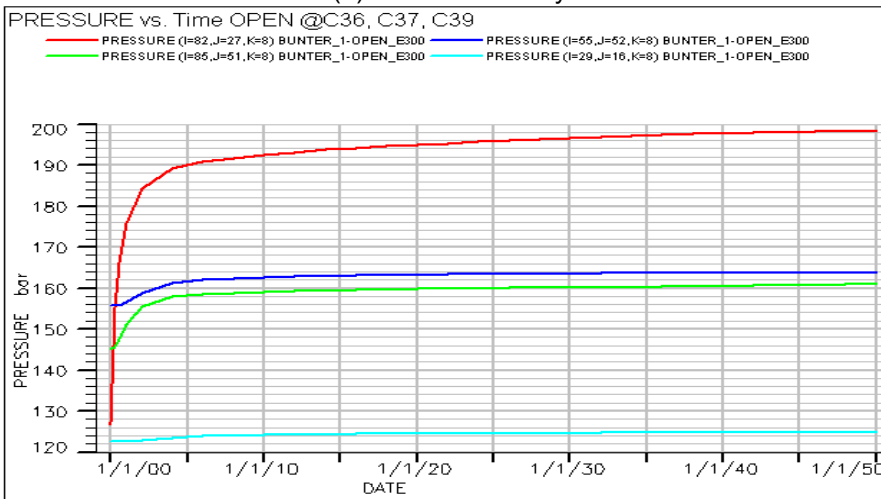
(c) open boundary

Figure A11.8: Pressure at the crest of Closure 36 (A – red), 37 (B – dark blue, C-green), and 39 (D – light blue) vs. time for base case (Zone 4 closed), model closed (middle), and open cases (bottom)

12 Dynamic Capacity Estimates and Sensitivity Studies

There is much uncertainty in the model properties, so it is unrealistic to give a single estimate of CO_2 storage capacity. Instead, a sensitivity study was carried out to estimate the range in potential capacity due to uncertainty in factors, such as the boundary condition and properties, and to calculate factors which can modify the base-case pore volume utilisation for use in different conditions. The factors include a sweep factor for different heterogeneous models (different vertical to horizontal permeability ratio K_v/K_h, and internal cement layers), volume/pressure factors, and simultaneous or sequential injection into several domes.

In previous studies of CCS (Bachu, Bonijoly et al. 2007), the effective storage volume V_{CO2e} for structural and stratigraphic traps was calculated by using the following equation:

$$V_{CO2e} = \eta \iiint \phi \left(1 - S_{wirr}\right) dxdydz = \eta \left(1 - S_{wirr}^*\right) PV \tag{12-1}$$

where $\eta = \eta_h \times \eta_b$ is the sweep efficiency that incorporates the cumulative effects of trap heterogeneity, CO_2 buoyancy and sweep efficiency; S_{wirr} is irreducible water saturation, and S_{wirr}^* is the pore volume weighted average irreducible water saturation. Note that we are assuming that the sweep efficiency is made up of two factors - a heterogeneity factor (subscript, h) and a buoyancy factor (subscript, b).

$$S_{wirr}^* = \left\{ \sum_{k=0}^{n} S_{wirr}^k PV^k \right\} \Big/ PV \tag{12-2}$$

The pore volume utilisation E then can be defined as:

$$E = \frac{V_{CO2e}}{PV} = \eta \left(1 - S_{wirr}^*\right) \tag{12-3}$$

12.1 Introduction to Sensitivity Cases

Six groups of sensitivity simulations were designed as shown in **Figure A12.1**. First, a sensitivity of well location relative to the height of the closure from the spill point to the crest was carried out in order to find the effect of injector location on capacity and to optimise the well location for the base-case. This has been described in Chapter 11. A total of four locations was chosen: at the crest (1200m in Closure 36), 1/5, 1/2 and 4/5 of the closure height (total relief = 1700m-1200m = 500m) from the crest, i.e. 1300m, 1450m, and 1600m, as shown in **Figure A11.4**. Ten injectors were located along the contour of the chosen depth for each case, except in the 1200m case in which only 9 wells were set in 9 cells at the top most locations. The monitor well was located on the crest cell which is near to the location of well 44/26-1 (442725, 5988942).

The second group of sensitivity cases was for the boundary condition sensitivity. The boundaries of the models were as follows:

A, B and C – these models were closed at the edges. The permeability in the cap rock is zero in Model A, 1.0×10^{-5} mD in Model B and 6.5×10^{-3} mD in Model C.

D (and base case) – these models were assigned the total pore volume of Zone 4 (280 km^3). The permeability of the caprock was 6.5×10^{-3} mD.

E – this model was closed around Closure 36.

Open – the total pore volume was set to 10,000 times the model's pore volume, to represent the fact that the Bunter Formation outcrops in the neighbourhood of the model (well 43/28a-3 is less than 20km away from the model). The field pressure in an open boundary model remains ideally constant.

Because of the difficulty in using analytical infinitely-sized aquifers with the Eclipse CO2STORE module, when dissolved CO_2 flowing is into the aquifer, a numerical aquifer was used in the open boundary cases. The model named "open-dyke" was designed for the case with possible dykes in the north-east and with salt walls in the south. The volume of the aquifers on each side of the model was altered to simulate the existence of the dyke and salt walls. Because of the lack of time, the analysis of the results is not included in this report. The last case in **Figure A12.1**, column 2, is a case with a constant injection rate assuming the site has a huge volume and a very good injectivity. This is an unrealistic situation in order to find the impact of flow rate to capacity when comparing with the results from other cases.

The third group was for testing the impact of injecting in one closure to the storage capacity of other neighbouring closures which are all in one 'parent' zone. There were two injection scenarios. One was the simultaneous injection case in which all storage closures were injected at the same time. The other was the sequential injection case, in which closures were injected one after another. The closure storage capacity was calculated and compared for the two different cases. Closure 36 was used as a storage site in the base-case and most of sensitivity study cases. The capacities of Closure 37 and Closure 39 were also estimated for both single- and multi-dome storage.

The next group of cases was to show the effect of heterogeneities, including the ratio of vertical permeability K_v to horizontal permeability K_h and the effect of the cement layer, followed by a sensitivity study of other factors, such as grid resolution and the uncertainty of the relative permeability curve, on the capacity estimation. Because of the limited time, this sensitivity study was set with a lower priority and only few cases were completed. A simulation of dome-fill injection followed by 1000 yr monitoring was set up. However, the CPU time for this scale (450,000 cells) was unaffordable (more than 1 month). It is unrealistic as a routine dynamic simulation without parallel computing facility.

The fifth group was for other sensitivity studies not included in the previous group. They showed the effect of fracture pressure gradient, relative permeability curves, and grid resolution on the estimation of storage capacity. This set of simulations included one run which was continued for 1000 years after injection. However, it was time consuming (>10 days).

The last group was required for economic modelling (WP3), and the results are described in Chapter 13. From the dynamic capacity calculation in the base case, the field injection rate must be less than 10 Mt/yr if the period of constant injection is about 50 years. A total of seven simulations were run, in which 3 closures (C36, C37 and C39) were used as storage sites for those cases where a field injection rate of more than 15 Mt/yr was required. The injectors in these cases were grouped for each closure. Group control was used for CO_2 injection, so that a constant rate could be maintained.

More than 100 dynamic simulations were run in the study within a limited time. The details of each case and the comparison of results is discussed in the following section. A full set of results is presented in **Table A12.1**.
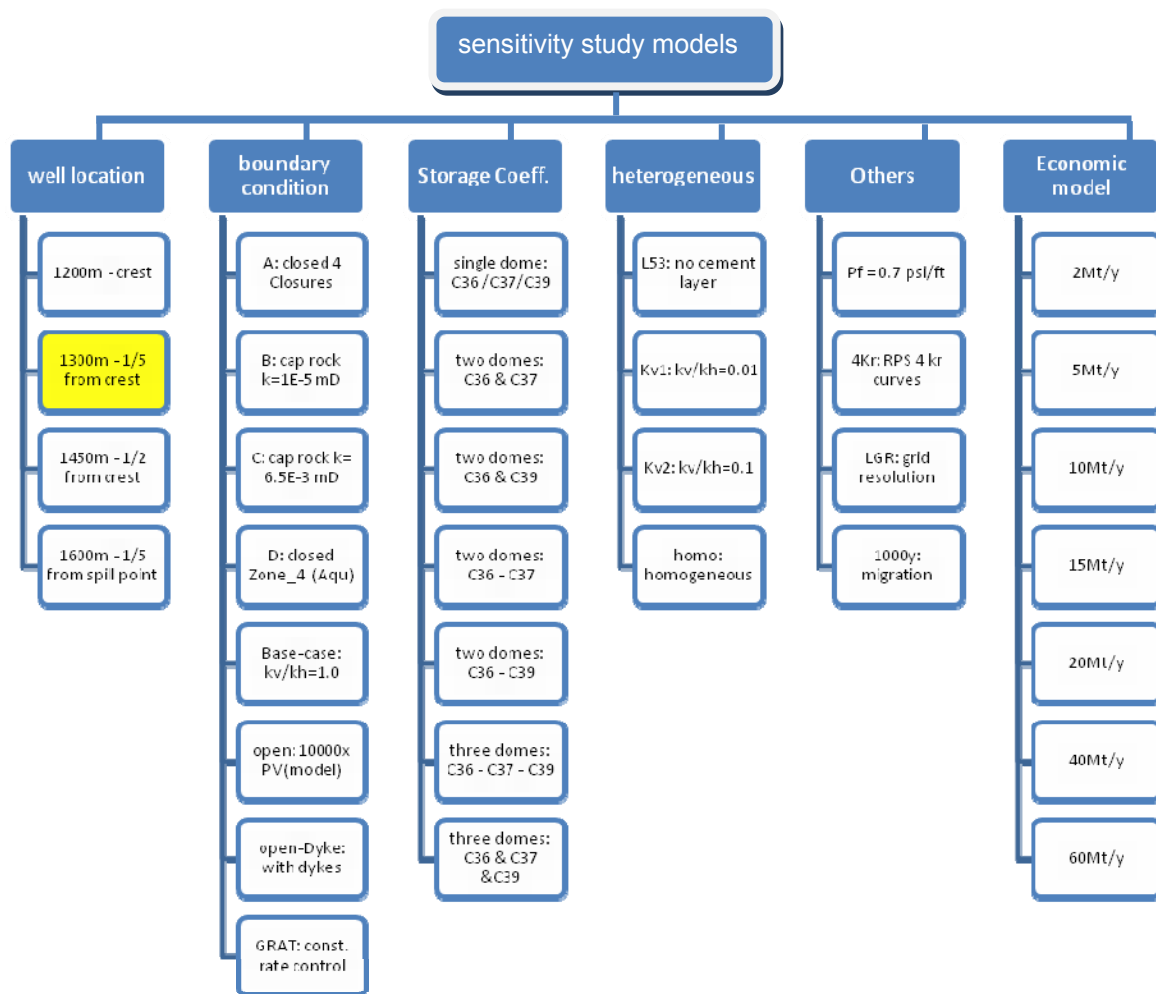

Figure A12.1: Sensitivity structure chart (base-case in yellow)

models	Zone_4 PV (x10^9 rm3)	dome PV (x1e6 rm3)			time of spillage (year)	Group gas injection total GGIT (x10^9 sm3)			Field PVU, E (%)	Dome PV Utilisation, E$_d$ (%)			PV weighted Ed	capacity (MT)	Sweep efficiency η (%)	Volume ratio (PV-brine/PV-dome)
		C36	C37	C39		C36	C37	C39		C36	C37	C39				
Base-case	280	2542			20				0.2	19.08				331	33.07	120.94
Bunter_1-A	39.6	2542			50				0.7	10.27				179	17.79	15.69
Bunter_1-B	39.6	2542			50				0.7	10.82				186	18.75	26.57
Bunter_1-C	39.6	2542			50				0.8	12.20				209	21.14	26.57
Bunter_1-D	280	2542			20				0.1	17.55				303	30.41	121.35
Bunter_1-E	12.2	2542			50				0.8	3.90				70	6.77	4.82
Bunter_1-	24293	2542			16				0.0	16.88				290	29.25	9467.91
KV1-0.01	280	2542			22				0.1	17.23				297	29.86	120.94
KV2-0.1	280	2542			20				0.1	17.55				303	30.41	120.94
L53 model	280	2542			26				0.2	24.51				426	42.48	120.94
HOMO	280	2542			42				0.2	32.80				484	56.83	134.35
4Kr	280	2542			10				0.1	11.05				191	19.78	120.94
GRAT	280	2542			16				0.2	18.37				318	31.48	120.94
HOM-W1200	280	2542			56				0.3	37.77				561	65.46	142.83
KV1-W1600	280	2542			12				0.1	7.44				127	12.89	120.94
1200m	280	2542			46				0.2	28.68				501	49.70	120.94
1450m	280				16				0.2	18.37				318	31.84	120.94
1600 m	280	2542			12				0.1	13.81				237	23.93	120.94
base-C37	280		3747		12	280	121		0.1		9.37				16.23	82.05
base-C39	280			3787	26	176	214		0.2			15.90			27.55	81.18
C36+C37	280	2542	3747		48	172		324	0.4	29.57	9.20		17.43	759	48.88	120.94
C36/C37	280	2542	3747		60	171		229	0.3	19.11	15.32		16.85	731	48.88	
C36+C39	280	2542		3787	58	268	126	295	0.4	18.27		22.95	21.07	916	48.58	120.94
C36+C39	24293	2542		3787	24	177	214	160	0.0	18.61		16.59	17.40	748	32.25	9467.91
C36+C37+C3	280	2542	3747	3787	100	280	121		0.6	27.87	9.10	20.54	18.14	1288	30.51	120.94
C36/C37/C39	280	2542	3747	3787	100	176	214		0.5	19.11	15.32	11.18	14.72	1030	30.51	120.94

Table A12.1: Pore volume utilisations calculated from dynamic modelling

12.2 Pore Volume Utilisation E_d and Sweep Efficiency η

The pore volume utilisation for Closure 36 can be derived in Eclipse (using Equation 12.1) from the ratio of volume of CO_2 injected to pore volume of Closure 36 (the volume between the top sandstone and the bottom sandstone, and surrounded by a polygon made from the depth contour at the spill point, 1730m).

The pore volume utilisation and capacity (in Mt) for different cases are listed in **Table A12.1**. The pore volume utilisation for the base case is 19.1% and the sweep efficiency $\eta = 0.33$ with $S^*_{wirr} = 0.423$ (calculated in Petrel, using Eq. 12.2). The normalised sweep efficiency factors, F, are shown in **Figure A12.2**, in which the factor for the base case is set to 1.0. We assume that this factor is composed of two factors, a buoyancy factor, $F_{\eta b}$, and a heterogeneity factor, $F_{\eta h}$. However, in reality, the effects of these factors are combined in a complex way, so in this report, the different factors effecting sweep efficiency were not explored further.

In calculating the minimum, most-likely and maximum values of pore volume utilisation and sweep efficiency we used the values determined in our sensitivity study as shown in **Figure A12.2**. For pore volume utilisation we took the base case as the most likely, the closed model (Bunter 1-E) as the minimum, and the homogeneous model (HOMO) as the maximum. However in the calculation of sweep efficiency, whilst the most likely value is again taken from the base case, the minimum and maximum values are from the two-variable combined sensitivity cases. The minimum sweep efficiency is taken from the case with wells at 1600m and kv=0.01, and the maximum is taken from the case with wells at 1200m and homogeneous case. The results are summarised in **Table A12.2**.

	Min	ML	Max
Pore Volume Utilisation (%)	4	19	33
Sweep Efficiency (%)	12	33	65

Table A12.2: Min, most-likely and max sweep efficiency

12.3 Multi-dome Injection and the Correlation between the Dome Pore Volume Utilisation and Number of Storage Domes in the Field/basin

If CO_2 storage is developed in the Bunter Formation, it is likely that there will be injection into multiple domes, and it is needed to determine how the storage in one dome is affected by injection into neighbouring domes. In the base case, only one dome was used as a storage site within Zone 4, and the ratio of model volume to dome volume was about 120.

Initially, the static capacity for multiple domes was assessed using two methods (Smith, Bentham et al. 2010): by treating Zone 4 as a closed system, or by treating each structural closure (dome) as independent.

Closed system

Zone 4 was assumed to be closed here. The maximum allowable pressure increase used by Smith et al (2010) was 0.75 of the average lithostatic pressure (0.75x12.33 MPa=9.25 MPa). However, Van der Meer (van der Meer and van Vees 2006) suggested using a pressure increase of 1 MPa at the basin scale, so 9.25 MPa seems risky.) Based on the compressibility averaged by UKSAP, and allowable pressure increase used by Smith et al (2010), the static pore volume utilisation for Zone 4 (Storage Unit ID=139.000 with the PV=$2.80x10^{11}$ m^2) (UKSAP 2010) is about 0.9% (Cr=$6.2x10^{-4}$ 1/MPa, C_w=$3.76 x10^{-4}$ 1/MPa and the density of CO_2 is 700kg/m^2), and the capacity is 1804 Mt. Here the data used in the calculation are all from UKSAP database for Zone 4, except an allowable pressure is from Smith et al because the average allowable pressure increase is even higher (10.62 MPa with 0.8xPf).

Open system with limited structural trapping

It was assumed that the structural trapping volume (total dome volume) is about 2% of total pore volume, and the maximum pore volume utilisation for each dome is 40%. The total pore volume of Zone 4 is 280km^3, and the density of CO_2 is approximately 700 Mt/km^3. Therefore, the capacity of Zone 4 is

280km^3 x 2% x 40% x 700 Mt/km^3 = 1568 Mt.

Comparing the open aquifer capacity with the closed aquifer capacity, it can be found that they are quite close. In the former case, in which the boundaries are assumed to be closed, the maximum allowable injection pressure limits the capacity. In the latter case, in which the boundaries are open to the sea, the spillage from each closure limits the capacity. In this exemplar model, the maximum storage capacity coefficient is about 30%. As discussed in Section 10.2, if 5.8% of Zone 4 PV can be used (10 Closures) and each closure can reach its best coefficient, then the storage capacity could be
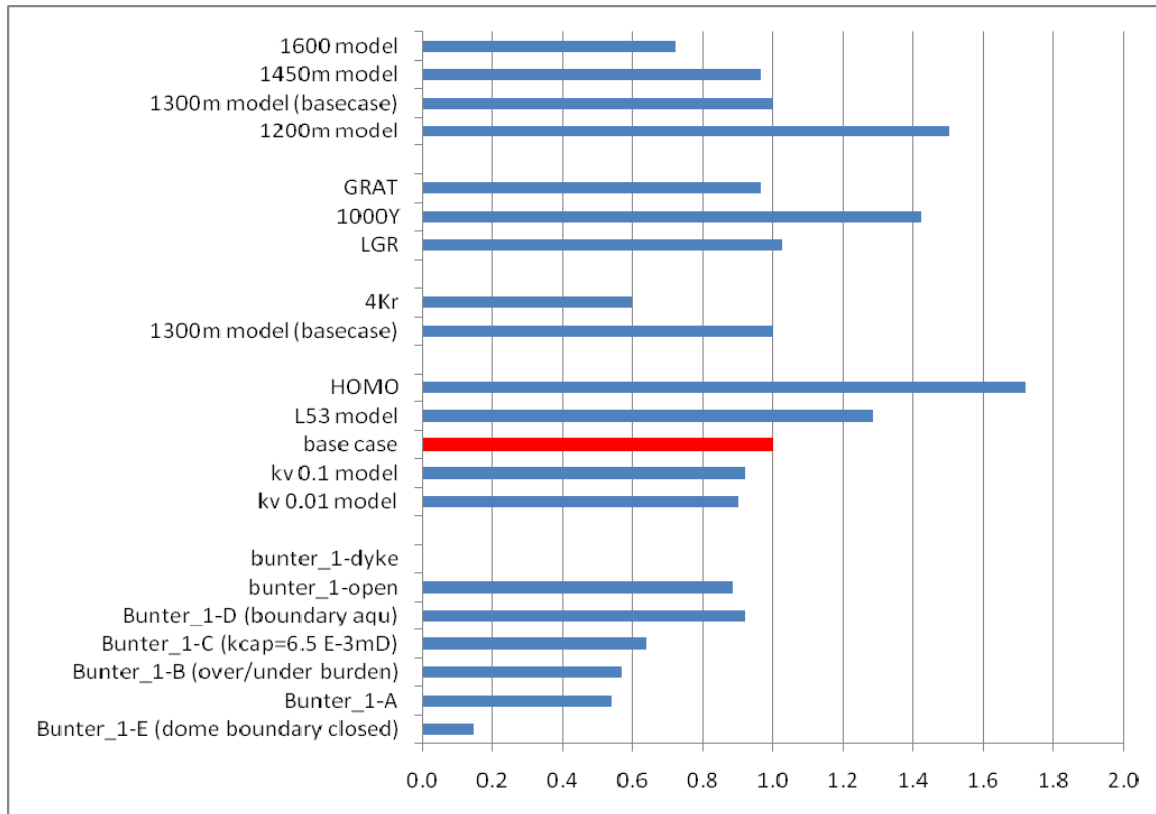
280km^3 x 5.8% x 30% x 700 Mt/km^3 = 3410 Mt.

Figure A12.2: Normalised sweep efficiency factor {$F_\eta = \eta/\eta_{base} = [E_d/(1-S_{wirr})]/[E_{db}/(1-S_{wirr-b})]$} for sensitivity cases, where E_d is the pore volume utilisation for any case, and E_{db} is the pore volume utilisation for base case, S_{wirr} and S_{wirr-b} are the saturation for any case and base, respectively

12.4 Dome PV Utilisation for Multi-dome Injection - Correlation with the Number of Domes

It takes tens of years for pressure recovery after stopping injection, based on this study. (The recovery time depends on the boundary conditions and on the pressure diffusivity, which is turn depends on the permeability, compressibility, etc.) Whether the system is open or closed, the pressure increase induced by injection in one dome will cause a pressure increase in the nearby neighbouring domes, and therefore affects the storage capacity of these domes. If the system is a closed one, the storage capacity of a dome depends on the ratio of the volume of a daughter dome and its parent volume. If the system is open, the buoyancy limited capacity should be used for each dome.

There were three closures used as storage sites in the Exemplar 2 model; these were C36, C37, and C39. The following injection scenarios were designed in the study to investigate the impact of multi-dome injection on the capacity of a single dome. As shown in **Figure A12.3**, the injection scenarios were divided into two groups, simultaneous or sequential, injecting into 2 or 3 domes. In each case, the wells were controlled by the bottom hole pressures of each injector and the monitoring well. The injectors in each closure remained open until the spillage criterion for the closure was exceeded. If the spillage criterion was not reached in a closure after 50 years of

injection, but the group injection rate had became very low due to the pressure control, the wells were also shut, and the capacity was calculated based on a maximum injection period of 50 years. The PV utilization for each dome in each case was calculated, and the results for the 2-dome and 3-dome cases were averaged, using the dome pore volume as a weighting factor. The calculated values are listed in **Table A12.1**.
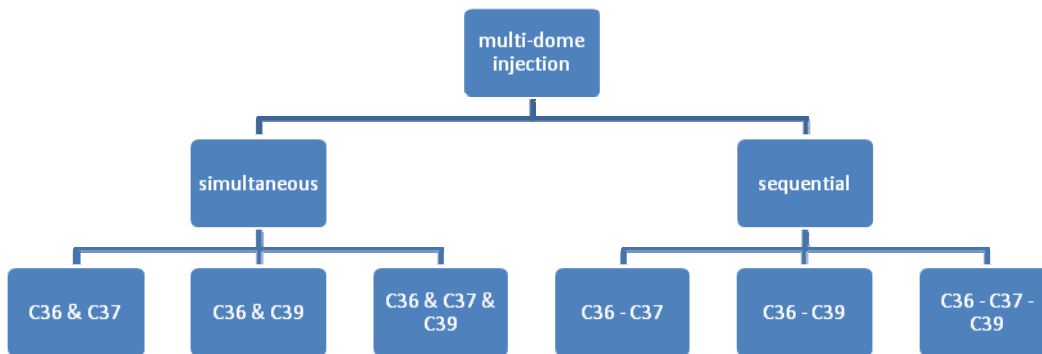

Figure A12.3: flow chart for multi-dome injection sensitivity study, C = Closure

As discussed before, the capacity of a closure depends on which parameter limits the injection: the injection pressure or spillage. In this study, when the fracturing pressure gradient was 0.016 MPa/m (0.7psi/ft), the dominant control in Closure 36 was pressure. However, when the fracturing pressure gradient was assumed to be 0.018 MPa/m (0.8 psi/ft), a higher pressure was allowed at the wells, and the simulation was no longer pressure-dominated, but was controlled by spillage. We refer to this case as buoyancy-dominated. (Note that the value assumed in the project was chosen as 0.8 psi/ft.)

12.5   The Impact of Boundary Conditions on Storage Capacity - Open Boundary vs. Closed Boundary

It is often thought that the highest closure storage capacity should be the one with an open boundary because there is no pressure constraint. However, our simulations do not show this. One of the reasons is because the formation is heterogeneous. The depositional environment for the Bunter Formation was interpreted as braided river channels with sheetflood and inter-bedded shale from petrel-zones 1 to 4 (Chapter 5 of this report). **Figure A12.4** shows the high permeability channels in the top layer of petrel-zone 4 that is under the cemented layer 53. CO_2 injected into the lower Bunter Sand will be blocked by the cemented layer and flow alone the channels toward SW or NE, as shown in **Figure A12.5**.

In the open boundary model, the local pressure increases slowly, so that injection rate remains high and CO_2 moves quickly along the channels without pressure confinement. The spillage criterion (defined as the ratio of total mass of CO_2 flowing out from Closure 36 to the total mass of

CO_2 injected), is reached before the dome is fully filled. **Figure A12.6** shows the change of spillage ratio with time for different cases in sensitivity study with the fracture pressure gradient equal to 0.016 MPa/m. It can be seen from the diagram that:

1. CO_2 flows toward the spill point much quicker in the case with open boundary, as shown in case 'open';

2. The closer the injector to the spill point, the slower the pressure at the crest increases, and therefore the sooner CO_2 reaches spill point (as shown in case 'w1450');

3. The less heterogeneous the model is, the less CO_2 moves toward spill point. Under buoyancy CO_2 moves more quickly towards the top rather than towards the spill point, in the homogeneous model and in the case without the cemented layer 53. Two patterns of spillage increasing with time can be seen in the diagram. One is a sharp increase. The other increases more slowly and reaches a maximum. (However, this maximum cannot be seen in **Figure A12.6**, because it occurs after 100 years.) The two types of variation reflect the two types of control - pressure and flow rate control during the injection.

The surprising result from the simulations in this study is that the storage in an open system may sometimes be less than that for a closed system. As can be seen in Table 12.1, the storage capacity for the open case (Bunter_1-) was 290 Mt, while the storage capacity for the base case was 331 Mt.
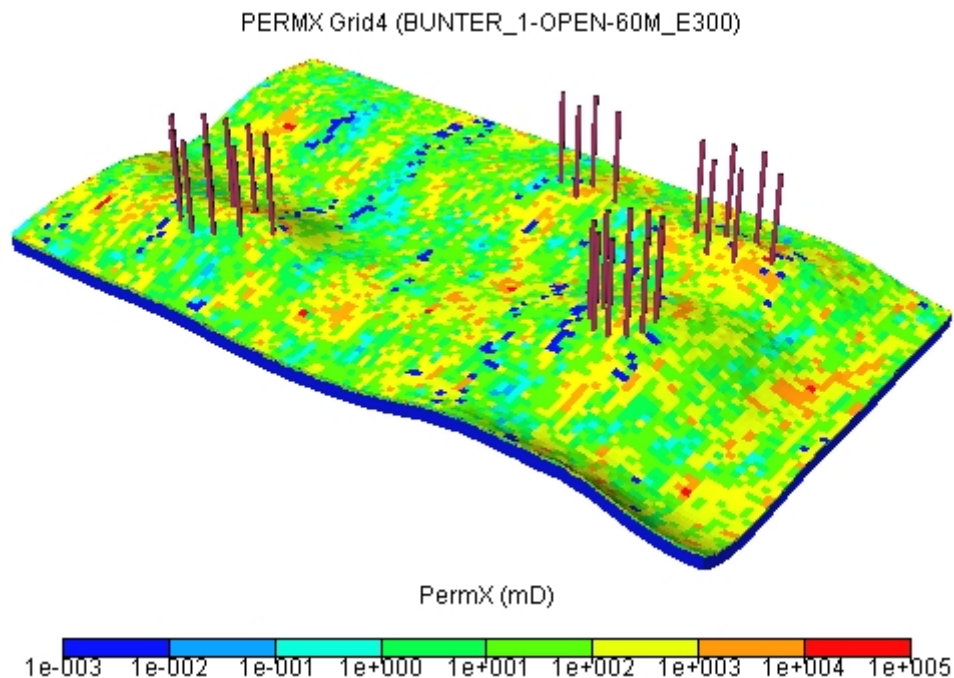
Figure A12.4: Permeability distribution in the Bunter model, top layer of petrel-zone 4; the channels run from SW to NE
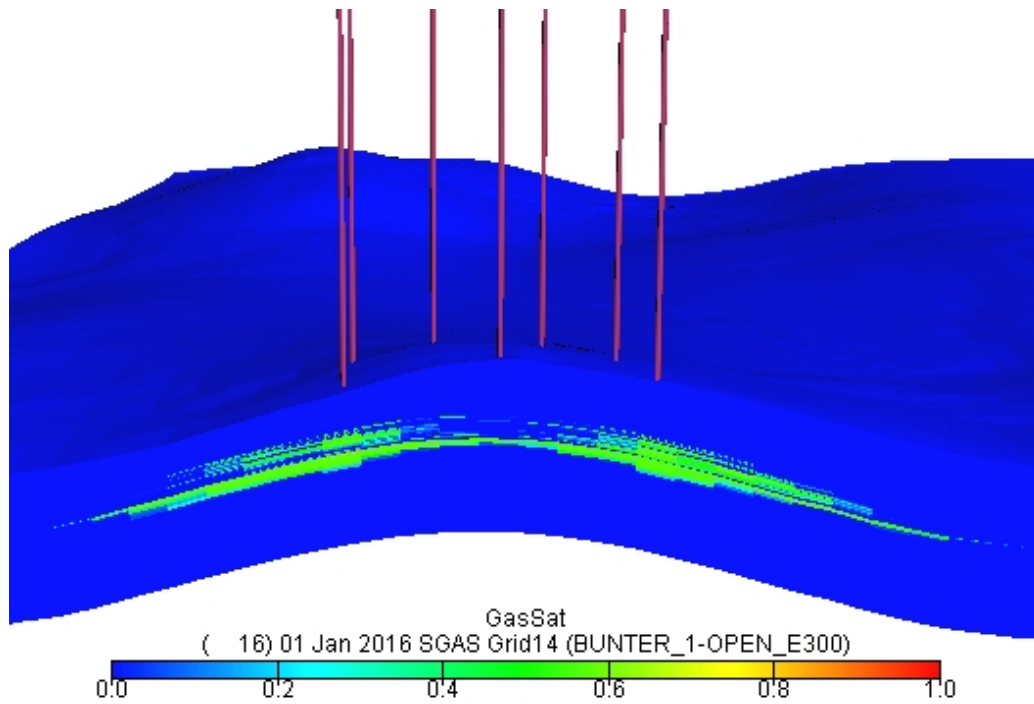
Figure A12.5: CO_2 saturation in the formation after 15 years injection shows the CO_2 migration along the sandstone formation. Because a cement layer divides the formation into upper and lower zones and the permeability of lower zone is much higher than that in upper zone, the movement of CO_2 in the lower zone is faster than that in the upper zone
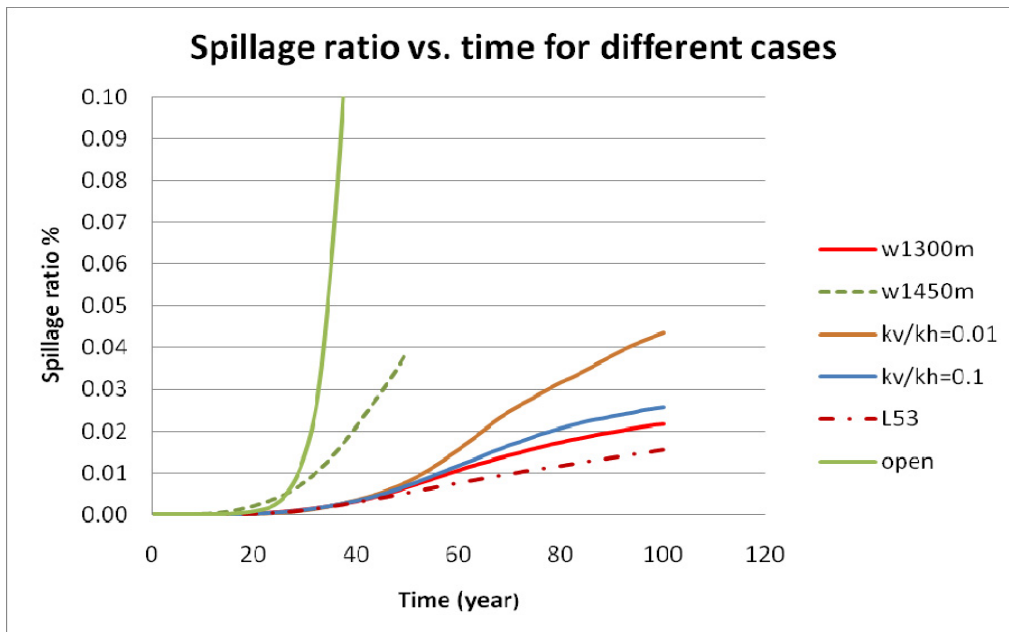
Figure A12.6: Total inter-region mass flow vs. time for open-boundary and closed-boundary cases

12.6   Impact of Heterogeneities on Storage Capacity

As discussed in Section 5.2.2 there is a cemented layer in the base case. The permeability of the layer is nearly zero, except in the vicinity of two drilled wells (49/01-3 and 43/22-1), as shown in **Figure A12.7** left. The vertical to horizontal permeability ratio k_v/k_h is 1.0 in the base case. In order to study the impact of geological heterogeneities on storage capacity, several sensitivity cases were designed with kv/kh = 0.1, 0.01, and with the permeability in Layer 53 equal to that in Layer 54. Additionally, a homogeneous model was set with porosity ϕ=0.15 and permeability k=100mD. The total pore volume of the homogeneous model was made similar to that of the base case model by adjusting the size of the numerical aquifers at the boundary of the model.

Figure A12.7: Permeability distribution of layer 53 in the base case (left - cemented sand layer) and sensitivity case without cemented layer (right); there are two holes at the cemented sand layer in base case
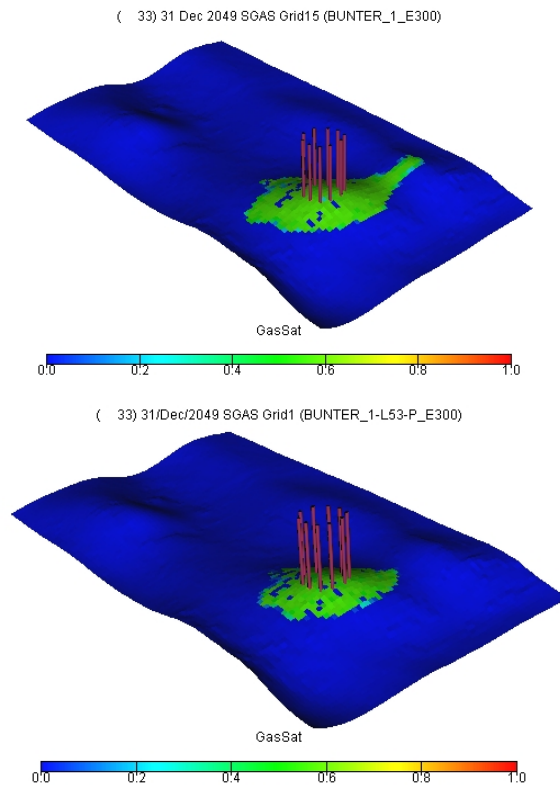
Figure A12.8: CO$_2$ saturation distribution in Layer 54 after 100 year injection from the base case (left) and the case without cemented layer (right);

It can be seen in **Figure A12.6** that the presence of the cemented layer (layer 53) has some effect. The sweep efficiency is increased by a factor about 1.3 when the layer is removed (case L53). Also the CO$_2$ migration route is different in the two cases (**Figure A12.8**). In the sensitivity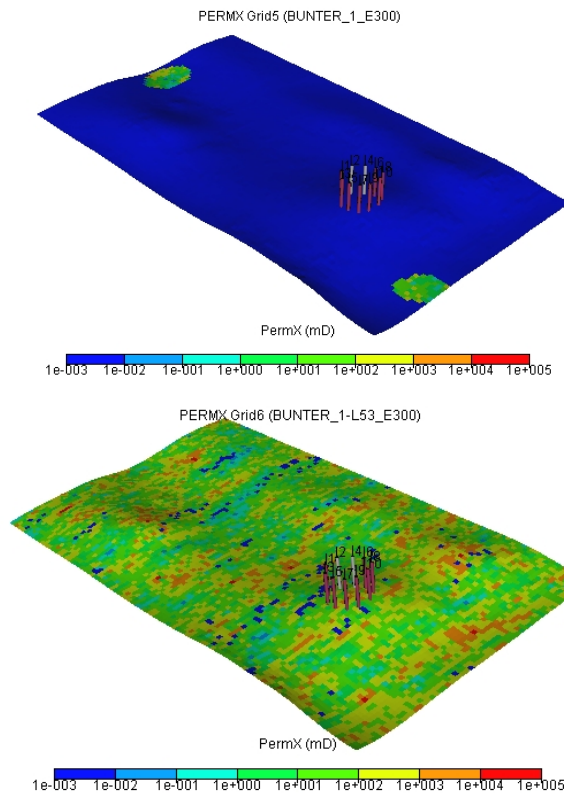 case (L53 - without the cemented layer - on the right), CO$_2$ was injected into the perforation below Layer 54 and could migrate through Layer 53 into upper Bunter Sand under the buoyancy. The CO$_2$ moved towards the crest first, and then moved down along the top layer of upper Bunter Sand (Layer 8). On the contrary in the base case, CO$_2$ injected in lower Bunter Sand migrated beneath the impermeable cemented layer. As a result, CO$_2$ in the base case reached the spill point sooner (58 years) than in the sensitivity case (70 years). However, compared with the sensitivity case, the cemented layer does not bring any dramatic change in pressure, as shown in **Figure A12.9**.

The storage capacity in the homogeneous case was the highest of all the sensitivity cases. The capacity decreases with the decrease in the value of k_v/k_h. It was found by comparing the field injection rate and the BHP at monitoring well that the lower k_v/k_h is, the more quickly the local pressure builds up. As a consequence, under the pressure control, the well injection rate reduces and less CO$_2$ is injected within a certain time. On the other hand, CO$_2$ moves laterally, rather than vertically, with lower k_v/k_h, so that less injection time is allowed for lower k_v/k_h case due to the spillage criterion.

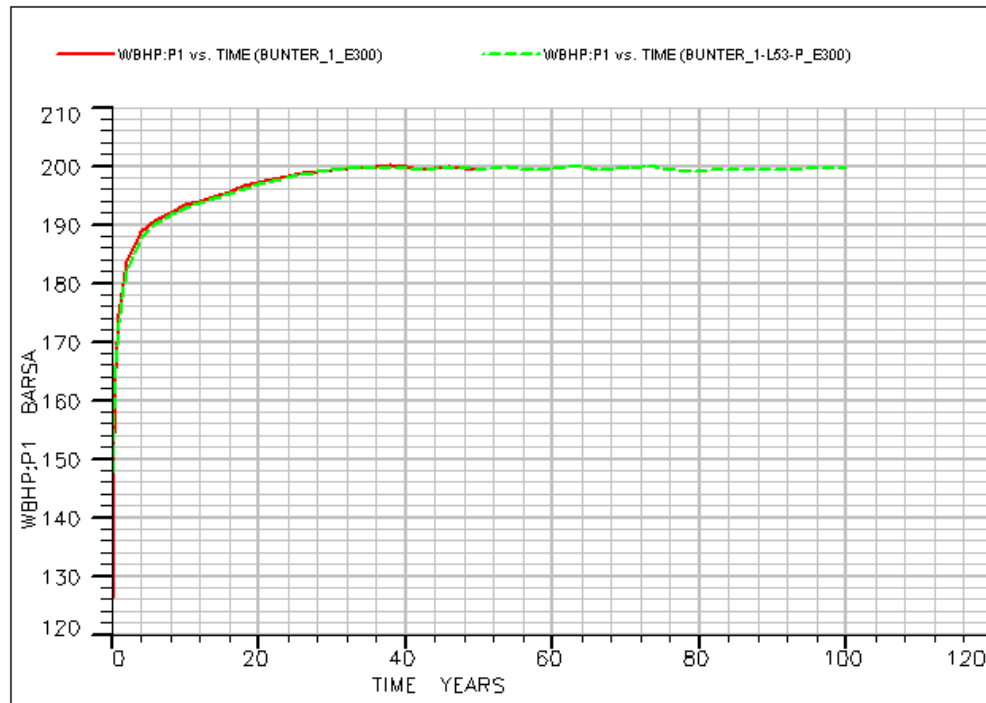**Figure A12.9: Pressure vs. time at the monitoring well for the base case and the case without cemented layer**

13   Simulations for Economic Modelling

A series of simulations was required for economic modelling. The main output was the WBHP under different injection rates (2, 5, 10, 15, and 20 Mt/yr) and at different times (1, 10, 20, 30, 40, and 50 years). In order to keep the injection rate relatively constant (requested by power plant or pipeline network), group control was used in the ECLIPSE model, with the wells being grouped according to closure. Beside the individual well control (maximum injection rate and BHP) and the pressure control by the monitoring well at the crest of Closure 36, a maximum injection rate, which depends on the capacity of each dome and a 50-year injection period, was defined for each group.

In the cases described in earlier sections of this report, the initial injection rate was set to 2 Mt/yr per well, so for 10 wells, the rate was 20 Mt/yr. However, with this rate, the pressure tended to build up and the rate was soon decreased. If a lower rate is used to start with, e.g. 1 Mt/yr, the required capacity (e.g. 500 Mt) may be achieved using a steady inject rate for the group. Using the group control, allows a higher injection rate in wells with good injectivity which compensates for a lower rate in wells with poor injectivity. **Table A13.1** lists the number of domes and wells used in each scenario.

The pressures listed in **Table A13.1** are the group-averaged WBHP and maximum THP at a given time corresponding to the injection rate required. Because no geomechanical coupled simulation results are available for the Exemplar_2 Bunter model, the number of well depends on the rule of thumb (<2.0 Mt/yr-well if the permeability is below 100 mD) and the results from base-case study.

Figure A13.1 shows field injection rate vs. time for the different economic models. As shown in the figure a constant field injection rate can be maintained for a total injection rate less than 10Mt/yr for 40 years in the one-dome injection plan. If the total injection rate is over 10Mt/yr, more domes/closures are required to keep the specified injection rate. If the total injection rate is over 40Mt/yr, the volume of Zone 4 is not large enough to maintain a constant injection rate for 40 years, so an open system is required. Actually the area under the injection curve shows the storage capacity of the closed system. **Figure A13.2** shows the field average pressure (FPR) vs. time for different models. It is interesting to note that whether the injection rate is 15Mt/yr, 20Mt/yr, or 40Mt/yr, the average pressure increase during the 50 years is similar (because of pressure constraints in the wells). The increase in pressure depends on the volume of reservoir and the total compressibility. It is also affected by the well pressure limits and the permeability.

It is very important to choose an appropriate value for the pressure increase value for static assessment of storage capacity, as the pressure required in the calculation is the average field pressure increase. For a dynamic estimation of storage capacity, the pressure limit is a bottom hole pressure, which depends on the strength of the cap rock and the strength of the rock near the wellbore. In this study, when the pressure limit at the wellbore is about 1.5 times of initial pressure (5.5-7.0 MPa), the field average pressure increase 3.4 MPa. Therefore, if a 9.25 MPa average pressure increase is allowed (Smith, Bentham et al. 2010) in a reservoir with moderate injectivity, the bottom hole pressure may increase more than 15 MPa. It is too high for a reservoir with average depth of 1600m unless the boundaries are open. This discussion raises the

question that when a boundary condition is uncertain for a storage site, capacity estimation may have a big range based on different assumptions.

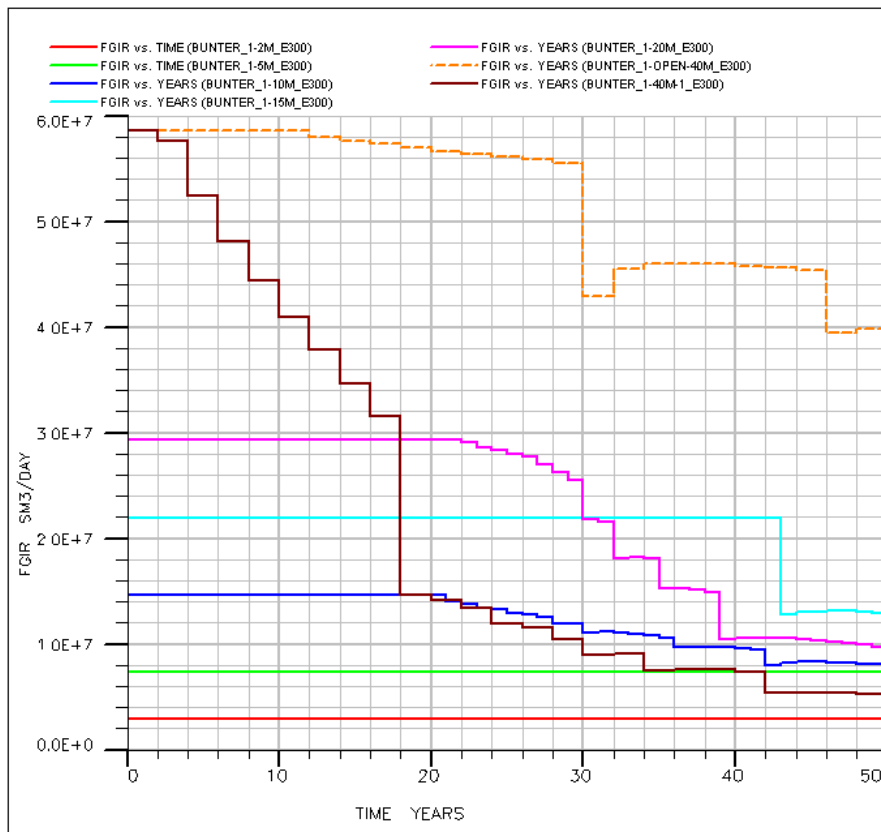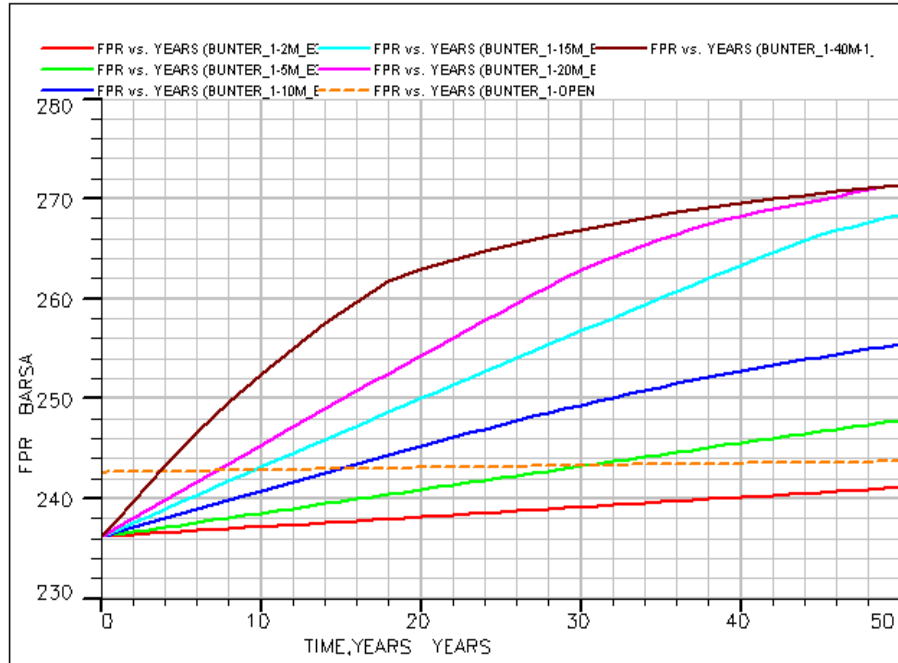**Figure A13.1: Simulated CO$_2$ injection rate vs time for different injection plan models**

Figure A13.2: Simulated field average pressure vs time for different injection plan models, in which only the orange dotted line is from an open boundary model

Rate	No. of wells	1 YEAR			10 YEARS			20 YEARS			30 YEARS			40 YEARS			50 YEARS		
		C36	C37	C39	C36	C37	C39	C36	C37	C39	C36	C37	C39	C36	C37	C39	C36	C37	C39
2Mt/y	2	169			162			163			164			165			166		
5Mt/y	3	168			169			172			174			177			180		
10Mt/y	10	174			184			189			195			200			205		
15Mt/y	3x10	161	180	159	170	188	166	177	196	172	184	203	179	190	209	185	196	216	191
20Mt/y	3x10	161	186	169	174	195	178	183	204	187	192	213	195	200	222	203	209	230	209
40Mt/y (open)	3x10	184	204	181	194	212	188	198	0	205	199	0	205	201	0	206	202	0	206

Rate	No. of wells	1 YEAR			10 YEARS			20 YEARS			30 YEARS			40 YEARS			50 YEARS		
		C36	C37	C39	C36	C37	C39	C36	C37	C39	C36	C37	C39	C36	C37	C39	C36	C37	C39
2Mt/y	2	97			88			89			90			92			93		
5Mt/y	3	86			87			90			94			98			101		
10Mt/y	10	79			91			98			104			111			117		
15Mt/y	3x10	48	65	43	59	75	51	68	84	59	76	92	67	83	101	75	90	109	83
20Mt/y	3x10	49	77	64	65	87	76	77	98	87	88	108	97	99	119	107	108	128	111
40Mt/y (open)	3x10	96	116	90	105	129	101	116	0	134	118	0	134	120	0	134	121	0	134

1. The pressure listed in the table is group average pressure of well bottom hole pressure (WBHP) or well tubing head pressure (WTHP).
2. pressure value '0' means that the well has been shut.

Table A13.1: Well Bottom Hole Pressure (WBHP) and Tubing Head Pressure (WTBH) vs. time for different injection rate. the numbers in columns 3 - 20 are pressure in bars

14 Discussion Summary of the Dynamic Simulations

The dynamic simulations showed a number of important findings, which are discussed below.

In the Bunter dome model, there were two types of control on CO_2 storage capacity. The first is pressure control. If the pressure increases too much, the injection rate must be reduced, leading to a lower storage capacity. We set a maximum pressure limit of 90% of the fracture pressure, which was calculated using a fracture pressure gradient of 0.8 psi/ft (=0.018 MPa/m). When the bottomhole pressure in a well reached this limit, the injector was switched to pressure control. The second control is rate control. If the pressure limit is not reached, the CO_2 injection rate is maintained. However, in this case, the CO_2 is free to migrate further. It will rise due to buoyancy until it reaches the caprock, or an impermeable layer within the aquifer, when it will migrate laterally and may reach a spill point. In our simulations, we stopped injection once 0.01% of the mass of injected CO_2 crossed a spill point, thus limiting the storage capacity. In practice, it may be impossible to determine whether or not this small percentage of CO_2 has migrated out of a dome. More research is required in this area from the point of view of simulation and CO_2 monitoring.

In the sensitivity study, two values for the fracture pressure gradient were tested: 0.7 psi/ft (0.016 MPa/m) and 0.8 psi/ft (0.018 MPa/m). It was found that the storage capacity and pore volume utilisation were very sensitive to the assumed fracture pressure gradient. The larger the assumed gradient, the higher the pressure is allowed to rise, and a high injection rate is maintained. This leads to rapid migration of CO_2 to the spill point. On the other hand, a low fracture pressure gradient, meant that the maximum pressure was reached at the wells more quickly, so the CO_2 injection was reduced, allowing it to rise buoyantly, and delaying the migration to the spill point.

It is usually assumed that the storage capacity in a closed system will be less than the capacity for an open system. However, this is not necessarily the case. In a heterogeneous model, the buoyant rise of CO_2 may be hampered by low permeability layers, and therefore reach the spill point sooner. The results of this study showed that heterogeneity significantly lowered the storage efficiency.

An observation well was placed at the crest of each dome where injection was taking place. It was found that, even though the pressure was constrained to be below the limit at the depth of the injector completions, the pressure at the crest of a dome could rise about the pressure limit. This implies that monitoring the pressure at the crest of a dome is important, so that there is no risk of breaching the seal at the crest.

The results of our simulations also indicate that is may be possible to increase storage capacity by controlling the ratio of viscous/gravity forces acting on the CO_2. If the injection rate is high (high viscous force), either the pressure will rise and the rate must be reduced, or if the pressure limit is not reached, the CO_2 may quickly migrate through a spill point. On the other hand, a lower injection rate (low viscous/gravity ratio), will encourage the buoyant raise of CO_2 and also dissolution in brine, increasing the storage capacity.

In summary, we determined that for the Bunter model studied, the most likely value of the pore volume utilisation, for injection into a single dome, was 19%. This is lower than some

previous estimates of 40%. However, there is much uncertainty in the models, and our sensitivity studies showed a large variation. The sweep efficiency ranged from 0.13 to 0.65, with a most likely value of 0.33.

15 References

1. Bachu, S., D. Bonijoly, et al. (2007). Estimation of CO2 storage capacity in geological madia - CSLF Phase 2 report. Task Force on co2 storage capacity estimation for the Technical Group (TG) of the carbon sequestration leadership forum (CSLF): 42.

2. Bentham, M., J. Williams, et al. (2011) Exemplar 2 - The Bunter Sandstone Formation Geocellular Model.

3. Bifani, R. (1986). Esmond Gas Complex. In Geological Society, London, Special Publications 1986; v. 23; p. 209-221

4. Brook, M., K. Shaw, et al. (2003). Gestco case study 2a-1: Storage potential of the Bunter Sandstone in the UK sector of the southern North Sea and the adjacent onshore area of Eastern England, British Geological Survey.

5. Cameron, T. D. J., Crosby. A., Baslon. P. S., Jeffery. D. H., Lott. G. K., Bulat. J and Harrison. D. J. (1992). United Kingdon Offshore Regional Report: the geology of the southern North Sea. British Geological Survey (London: HMSO for the British Geological Survey)

6. Chadwick, A., Arts, R., et al., (2008) Best practice for the storage of CO_2 in saline aquifers – Observations and guidelines from the SACS and CO2STORE projects, British Gellogical Survey

7. DECC (2011 updated). Department of Energy and Climate Change.

8. Deegan, C.E. and Scull, B.J. 1977. A standard lithostratigraphic nomenclature for the Central and Northern North Sea. Institute of Geological Sciences Report No. 77-25, 36 pp.

9. Downing, R. A., D. J. Allen, et al. (1985). Cleethorpes No. 1 Geothermal Well - a preliminary assessment of the resource. Keyworth, British Geological Survey.

10. Evans, D., Graham, C., Armour, A. and Bathurst, P. 2003. The Millennium Atlas: Petroleum Geology of the Central and Northern North Sea, Geological Society of London, 389 pp.

11. Glennie, K. W (editor). (1998) Petroleum Geology of the North Sea. Basic concepts and recent advances. Fourth Edition.

12. Holloway, S. (2010). Modelling CO2 injection into the Bunter Sandstone (an update on work in progress), BGS.

13. Holloway, S., Bentham, M., Kirk, K., Williams, J., Wilkinson, M. and Scott, D. (2011). UK Storage Appraisal Project Milestone 1.9 Report. The Energy Technologies Institute.

14. Ketter, F. J. (1991). The Esmond Forbes and Gordon Fields, Blocks 43/8a, 43/13a, 43/15a, 43/20a, UK North Sea. *From* Abbotts, I. L. (ed), 1991, United Kingdon Oil and Gas Fields, 25 Years Commemorative Volume, Geological Society Memoir No. 14, pp.425-432.

15. Pickup, G. E. , Kiatsakulphan, M. and Mills, J. R., 2010. "Analysis of grid Resolution for Simulations of CO2 Storage in Deep Saline Aquifers", paper A021, presented at the 12th European Conference on the Mathematics of Oil Recovery, Oxford, UK, 6 - 9 September, 2010.

16. Raistrick, M., Bentham, M., Daniels, S., Jenkins, S. and Wilkinson, M. (2011). UK Storage Appraisal Project Work Package 2 Full Report. The Energy Technologies Institute.

17. Ritchie, J. S and Pratsides, P. (1993). The Caister fields, Block 44/23a, Uk North Sea. *From* Petroleum Geology of Northwest Eurpoe: Proceedings of the 4th Conference (edited by J. R. Parker). Pp 759-769.

18. Schlumberger (2010). ECLIPSE Reference Manual. 2010.1.

19. Smith, D. J., M. Bentham, et al. (2010). The impact of boundary conditions on CO_2 capacity estimation in aquifers. 9th Annual conference on carbon capture and sequestration.

20. Spain, D. R and Conrad, C. P. (1997). Quantitative analysis of top-seal capacity: Offshore Netherlands. southern North Sea. In Geologie en Mijnbouw 76, pp 217-226.

21. UKSAP (2010). UKSAP web application.

22. van der Meer, L. G. H. and J. D. van Vees (2006). Limitations of the storage pressure in finite saline aquifers and the effects of the CO_2 solubility on the storage pressure, SPE 103342.

23. White, D.A. 1998. Oil and gas play maps in exploration and assessment. AAPG Bull., 72, 944-949.

24. Williams, J. (2011). Bunter_exemplar_area_V2_EJMresponse.ppt.

25. Williams, J. and M. Bentham (2011). Exemplar 2, the Bunter Sandstone Formation. Keyworth, British Geological Survey.

26. Bachu, S., D. Bonijoly, et al. (2007). Estimation of CO_2 storage capacity in geological madia - CSLF Phase 2 report. Task Force on co2 storage capacity estimation for teh Technical Group (TG) of the carbon sequestration leadership forum (CSLF): 42.

27. Brook, M., K. Shaw, et al. (2003). Gestco case study 2a-1: Storage potential of the Bunter Sandstone in the UK sector of the southern North Sea and the adjacent onshore area of Eastern England, British Geological Survey.

28. Downing, R. A., D. J. Allen, et al. (1985). Cleethorpes No. 1 Geothermal Well - a preliminary assessment of the resource. Keyworth, British Geological Survey.

29. Holloway, S. (2010). Modelling CO_2 injection into the Bunter Sandstone (an update on work in progress), BGS.

30. Smith, D. J., M. Bentham, et al. (2010). The impact of boundary conditions on CO_2 capacity estimation in aquifers. 9th Annual conference on carbon capture and sequestration.

31. Smith, D. J., M. Bentham, et al. (2010) The impact of boundary conditions on CO_2 storage capacity estimation in aquifers. GHGT-10

32. UKSAP (2010). UKSAP web application.

33. van der Meer, L. G. H. and J. D. van Vees (2006). Limitations of the storage pressure in finite saline aquifers and the effects of the CO_2 solubility on the storage pressure, SPE 103342.

34. Williams, J. and M. Bentham (2011). Exemplar 2, the Bunter Sandstone Formation. Keyworth, British Geological Survey.